Calculation of electron-helium scattering

Dmitry V. Fursa and Igor Bray*

Electronic Structure of Materials Centre, The Flinders University of South Australia,
G.P.O. Box 2100, Adelaide 5001, Australia

We present the convergent close-coupling theory for the calculation of electron-helium scattering. We demonstrate its applicability at a range of projectile energies of 1.5 to 500 eV to scattering from the ground state to $n \leq 3$ states. Generally good agreement with experiment is obtained with the available differential, integrated, ionization, and total cross sections, as well as with the electron-impact coherence parameters up to and including the $3\,^3D$-state excitation. This agreement is shown to be overall the best of the currently used electron-helium scattering theories. On occasion, some significant discrepancies with experiment are observed, particularly for the triplet-state excitations.

I. INTRODUCTION

The convergent close-coupling (CCC) method for electron-hydrogen scattering was introduced by Bray and Stelbovics [1]. It was developed in response to the long-standing discrepancies between the measured and calculated angular correlation parameters for this most fundamental electron-atom scattering problem. The CCC method was unable to resolve the discrepancy with experiment. However, as it solves the full nonrelativistic three-body problem to a demonstrated precision (convergence), there is no more that we can do to improve the theory for this scattering problem, and we take the view that in this case theory is likely to be more accurate than experiment. It is ironic that the success of the CCC method was not demonstrated on the problem which provided considerable motivation for its development, but in many other diverse applications.

The CCC method relies on the close-coupling (CC) formalism for solving the coupled equations without approximation. Convergence is tested by including an ever increasing set of target states in the CC formalism. The target states are obtained by diagonalizing the target Hamiltonian in an orthogonal Laguerre basis. The usage of such bases ensures that completeness is approached as the basis size is increased. The square integrability of the basis ensures that both the negative and positive energy states are square integrable, with the former converging pointwise to the true eigenstates with increasing basis size, while the latter provide a discretization of the target continuum. The treatment of both the discrete and continuum parts of the target space via the CC formalism allows the validity of the CCC method to be independent of the projectile energy or the transition of interest.

As we are only interested in developing general scattering theories we value very highly any test that may invalidate the CCC method. In our view the most fundamental test is provided by the application to the Temkin-Poet model [2,3], which simplifies the electron-hydrogen scattering problem by treating only states with zero orbital angular momentum, and has been solved to a high accuracy in a broad energy range. Application of the CCC method to this problem [4] demonstrated that, as the Laguerre basis size was increased, the results converged to the correct values at all energies. Pseudoresonances, typically associated with square-integrable representations of the continuum, diminish and disappear with increasing basis size. For a detailed example of this effect near a fixed pseudothreshold, see Ref. [5]. We consider this model problem to be very important and have provided an extensive set of tabulated results for this case [6].

Another important test of the method is provided by the calculation of total ionization cross sections and spin asymmetries for electron impact of atomic hydrogen [7]. This demonstrated that electron flux was distributed correctly between the independent singlet and triplet ionization channels, thus validating the treatment of exchange and the use of discretization of the continuum. In fact we may readily use the CCC method to calculate reliably $(e, 2e)$ differential cross sections [8].

The CCC method has been generalized to include hydrogenic atoms and ions as targets [9]. These are those targets for which the frozen-core Hartree-Fock approximation yields relatively accurate target states. Perhaps the most conclusive demonstration of the reliability of the CCC method, prior to the current work, was the ability to obtain quantitative agreement with almost all of the available spin-resolved measurements in electron-sodium scattering [9]. It was demonstrated that correct results for the simple, though spin-resolved, $3S$-$3S$ and $3S$-$3P$ transitions were, on occasion, only possible if the target continuum was treated very accurately. In our view the remarkable success of the CCC method for the sodium target is due primarily to the correct description of the electron-hydrogen scattering system. A summary of applications of the CCC method to electron scattering on hydrogenic targets may be found in Ref. [10].

*electronic address: igor@esm.ph.flinders.edu.au

We now turn our attention to the electron-helium scattering problem. Over recent years it has become apparent that the status of theory for this problem is considerably worse than that in the case of hydrogenic targets. What seems to us as the most fundamental cross section, namely, the elastic, is unable to be described by most theories. This is because a large proportion of the target polarizability is due to the target continuum. As far as we are aware, of the currently used theories only the coupled-channels optical (CCO) theory [11,12] includes an approximate treatment of the continuum. This is sufficient to get very good elastic cross sections, but a number of approximations in the CCO theory make it less reliable for the triplet transitions. An early application of the R-matrix theory [13] included a single pseudostate which was sufficient to give good elastic cross sections.

By treating many discrete target eigenstates (up to 29) via the R-matrix method Fon et al., [14,15] hope to get good results for the inelastic transitions at energies not far above the ionization threshold. These calculations do not attempt to treat the target continuum, and so do not obtain correct elastic cross sections. Nevertheless, such calculations have dominated applications to electron-helium scattering since the late 1970s.

There are also perturbative methods available. These include the distorted-wave Born approximations (DWBA) of Bartschat and Madison [16] and first-order many-body theory (FOMBT) of Cartwright and Csanak [17]. These usually give a good description of $n\,^1P$ excitation, but are less reliable for some of the other transitions, and are primarily high energy approximations.

Our aim is to provide a single electron-atom and -ion scattering theory that will yield reliable results for all transitions of interest including elastic, excitation, ionization, and total cross sections for energies below 1 keV. At higher energies the Born approximation provides a more computationally efficient way of generating electron scattering information. Having achieved this for hydrogenic targets we now demonstrate this for the helium target.

This work is structured in the following way. In Sec. II we give the formalism for generating the helium target states to be used in the close-coupling formalism. In Sec. III we present the CCC theory for the calculation of electron-helium scattering. This is followed by an extensive results Sec. IV. In subsection IV A differential cross sections for excitation of the ground state to $n \leq 3$ states are given at an energy range of 1.5 to 500 eV. In the following subsection IV B we give the integrated, ionization, and total cross sections. In subsection IV C the electron-impact coherence parameters (EICP's), as defined by Andersen, Gallagher, and Hertel [18], are presented for the $n\,^{1,3}P$ and $3\,^{1,3}D$ states whenever there are available measurements. In Sec. V we draw conclusions arising from this work and indicate future directions for our research.

II. CALCULATION OF HELIUM TARGET STATES

The nonrelativistic helium target Hamiltonian H_T can be written as

$$H_T = H_1 + H_2 + V_{12}, \tag{1}$$

where

$$H_i = K_i + V_i = -\frac{1}{2}\nabla_i^2 - Z/r_i, \tag{2}$$

for $i = 1, 2$, is the one-electron Hamiltonian of the He$^+$ ion ($Z = 2$), and

$$V_{12} = 1/|\boldsymbol{r}_1 - \boldsymbol{r}_2| \tag{3}$$

is the electron-electron potential. Atomic units are assumed throughout.

We use the L-S coupling scheme, and so the helium wave functions $\Phi^{ls\pi}$ are characterized by the orbital angular momentum l, spin s, and parity π. For each combination of $ls\pi$ we diagonalize the target Hamiltonian (1) in an antisymmetrized two-electron basis. One-electron orbitals $\varphi_\alpha(x)$, which are used to build the two-electron basis, are a product of a radial function, a spherical harmonic, and a spin function ($\sigma = \pm 1/2$)

$$\varphi_\alpha(x) = \frac{1}{r}\phi_{k_\alpha l_\alpha}(r)Y_{l_\alpha m_\alpha}(\hat{\boldsymbol{r}})\chi(\sigma). \tag{4}$$

Here x is used to denote both the spatial and spin coordinates. The radial part of the single-particle functions we take to be the Laguerre basis

$$\phi_{kl}(r) = \left(\frac{\lambda_l(k-1)!}{(2l+1+k)!}\right)^{1/2}$$
$$\times (\lambda_l r)^{l+1}\exp(-\lambda_l r/2)L_{k-1}^{2l+2}(\lambda_l r), \tag{5}$$

where the $L_{k-1}^{2l+2}(\lambda_l r)$ are the associated Laguerre polynomials, and k ranges from 1 to the basis size N_l.

For brevity of notation we denote helium states by $\Phi_n(x_1, x_2)$, where $n = 1, \ldots, N$, with corresponding orbital angular momentum $l = l_n$, spin $s = s_n$, and parity $\pi = \pi_n$, and which may be written as

$$\Phi_n(x_1, x_2) = \sum_{\alpha,\beta} C_{\alpha\beta}^{(n)}|\varphi_\alpha(x_1)\varphi_\beta(x_2) : \pi_n l_n m s_n \nu\rangle. \tag{6}$$

Here the configuration interaction (CI) coefficients $C_{\alpha\beta}^{(n)}$ satisfy the symmetry property

$$C_{\alpha\beta}^{(n)} = (-1)^{l_\alpha+l_\beta-l_n-s_n}C_{\beta\alpha}^{(n)} \tag{7}$$

to ensure antisymmetry of the two-electron target states. The two-electron functions in (6) are

$$|\varphi_\alpha(x_1)\varphi_\beta(x_2) : \pi l m s \nu\rangle$$
$$= \frac{1}{r_1 r_2}\phi_{k_\alpha l_\alpha}(r_1)\phi_{k_\beta l_\beta}(r_2)|l_\alpha l_\beta : lm\rangle X(s\nu), \tag{8}$$

where $\pi = (-1)^{l_\alpha+l_\beta}$,

$$|l_\alpha l_\beta : lm\rangle = \sum_{m_\alpha,m_\beta} C_{l_\alpha l_\beta l}^{m_\alpha m_\beta m_l}Y_{l_\alpha m_\alpha}(\hat{\boldsymbol{r}}_1)Y_{l_\beta m_\beta}(\hat{\boldsymbol{r}}_2), \tag{9}$$

and the two-electron spin function is defined by

$$X(s\nu) = \sum_{\sigma_1,\sigma_2} C^{\sigma_1\sigma_2\nu}_{\frac{1}{2}\frac{1}{2}s} \chi(\sigma_1)\chi(\sigma_2). \tag{10}$$

The target states $\Phi_n(x_1, x_2)$ satisfy

$$\langle \Phi_{n'} | H_T | \Phi_n \rangle = \epsilon_n \delta_{n'n}, \tag{11}$$

where ϵ_n is the energy associated with $\Phi_n(x_1, x_2)$. Some of the $\Phi_n(x_1, x_2)$ will be true discrete eigenstates, others will be a discrete representation of the target continuum. As the basis sizes N_l are increased the lowest in energy states converge to the true eigenstates, whereas the positive energy states provide an increasingly dense discretization of the continuum.

Whereas the above formalism is general and includes two-electron excitation, in practice we have found that it is sufficient to make the frozen-core approximation, in which all configurations have one of the electrons occupying the lowest orbital. In order to get a good description of both the ground and excited states we take $\lambda_0 = 4$ for $k = 1$ in (5). This choice generates the He$^+$ 1s orbital, which allows us to take into account short-range correlations in the ground state, as well as being able to obtain an accurate representation of a number of excited discrete eigenstates. To obtain an approximately equal number of negative and positive $^{1,3}S$ excited states we take $\lambda_0 = 1.25$ for $k > 1$. Choosing such λ_0 leads to a nonorthogonal basis. This results in the minor complication of having to solve the generalized eigenvalue problem. For all other $^{1,3}L$ states, we take the same λ_l for all k. For P states we take $\lambda_1 \approx 1$, for D and F states we take $\lambda_2 \approx \lambda_3 \approx 0.7$. The resulting frozen-core model (FCM) energies for $n \leq 4$ states are given in Table I. These are compared with experiment and the energy levels used in the 19-state R-matrix calculations [19]. Even

TABLE I. One-electron ionization energies (eV) of the $n \leq 4$ helium states calculated in the frozen-core model (FCM), and the configuration interaction model (R19) as used in the 19-state R-matrix calculation [19]. The experimental values are due to Moore [34].

State	FCM	R19	Experiment
1^1S	23.736	23.315	24.58
2^3S	4.740	4.740	4.767
2^1S	3.901	3.900	3.971
2^3P	3.573	3.573	3.622
2^1P	3.332	3.328	3.368
3^3S	1.864	1.858	1.868
3^1S	1.648	1.645	1.666
3^3P	1.567	1.567	1.580
3^3D	1.512	1.512	1.513
3^1D	1.512	1.512	1.513
3^1P	1.490	1.488	1.500
4^3S	0.989	0.974	0.993
4^1S	0.901	0.871	0.914
4^3P	0.874	0.870	0.879
4^3D	0.851	0.851	0.851
4^1D	0.850	0.850	0.851
4^3F	0.850	0.850	0.850
4^1F	0.850	0.850	0.850
4^1P	0.841	0.841	0.845

though the latter used a complex configuration interaction expansion we find our energy levels to be generally a little better for all excited states and significantly better for the ground state. Our results for the energies and oscillator strengths are consistent with the early work of Cohen and Kelly [20] and Cameron, McEachran, and Cohen [21].

III. CALCULATION OF ELECTRON-HELIUM SCATTERING

A helpful feature of the CCC formalism is that the derivation of the coupled equations and the method of solution are essentially independent of the choice of the target, and are similar to those given for hydrogenic targets [9]. We will not concentrate our attention on these issues here, but give a general outline. However, the calculation of the V-matrix elements for the helium target is very much more complicated than that for hydrogenic targets [10], and will be given in some detail.

A. The coupled equations for the T matrix

The total energy E, Hamiltonian H, and wave function $|\Psi\rangle$ with outgoing spherical wave boundary conditions are related by

$$0 = (E^{(+)} - H)|\Psi\rangle = (E^{(+)} - H_T - H_0 - V_{01} - V_{02})|\Psi\rangle, \tag{12}$$

where the 0 index is used to denote the projectile space, with the 1 and 2 indices being used for target space. To solve this equation, we write $|\Psi\rangle$ as an explicitly antisymmetrized wave function utilizing the multichannel expansion

$$\Psi^N(x_0, x_1, x_2) = (1 - P_{01} - P_{02})\psi^N(x_0, x_1, x_2) \tag{13}$$

$$= (1 - P_{01} - P_{02}) \sum_{n=1}^{N} \Phi_n(x_1, x_2) f_n^N(x_0), \tag{14}$$

where $P_{0\alpha}$ is the space (coordinate and spin) exchange operator. In the CCC method we rely on the completeness of the Laguerre basis so that

$$\lim_{N\to\infty} \Psi^N(x_0, x_1, x_2) = \Psi(x_0, x_1, x_2). \tag{15}$$

A discussion regarding the nonuniqueness of the expansion (14) will be given in a separate subsection.

Substitution of (13) into (12) results in

$$(E^{(+)} - K_0 - U_0 - H_T)\psi^N(x_0, x_1, x_2)$$
$$= V\psi^N(x_0, x_1, x_2), \tag{16}$$

where

$$V = V_0 - U_0 + V_{01} + V_{02} + (E - H)(P_{01} + P_{02}), \tag{17}$$

and the limit of large N is implicit. This rearrangement is such that the asymptotic (large r_0) Hamiltonian is $K_0 + U_0 + H_T$, and this will be used to generate the Green's function and boundary conditions for the total wave function

$$\lim_{r_0 \to \infty} \Psi(x_0, x_1, x_2) = \chi(\sigma) \exp(i\mathbf{k}_i \cdot \mathbf{r}_0) \Phi_i(x_1, x_2), \quad (18)$$

where $\mathbf{k}_i$ is the incident projectile momentum and Φ_i is the initial target state. In the CCC method we usually solve the coupled equations using a distorted-wave formalism [9]. This allows the use of arbitrary short-ranged potentials U_0, which are used purely as numerical techniques for reducing the required computational resources in solving the coupled equations.

We define the T matrix to be

$$\langle \mathbf{k}_f^{(-)} \Phi_f | T^N | \Phi_i \mathbf{k}_i^{(+)} \rangle = \langle \mathbf{k}_f^{(-)} \Phi_f | V | \psi^N \rangle, \quad (19)$$

where the distorted waves (discrete or continuous) $|\mathbf{k}^{(\pm)}\rangle$ satisfy

$$(\varepsilon_k^{(\pm)} - K_0 - U_0)|\mathbf{k}^{(\pm)}\rangle = 0. \quad (20)$$

The on-shell momenta $\varepsilon_k = k_n^2/2$ are obtained from

$$E - \epsilon_n - k_n^2/2 = 0, \quad (21)$$

and exist only for open channels n such that $E = \epsilon_i + k_i^2/2 > \epsilon_n$.

The coupled Lippmann-Schwinger equations for the distorted-wave T matrix are [9]

$$\langle \mathbf{k}_f^{(-)} \Phi_f | T^N | \Phi_i \mathbf{k}_i^{(+)} \rangle = \langle \mathbf{k}_f^{(-)} \Phi_f | V | \Phi_i \mathbf{k}_i^{(+)} \rangle + \sum_{n=1}^{N} \sumint_{k} \frac{\langle \mathbf{k}_f^{(-)} \Phi_f | V | \Phi_n \mathbf{k}^{(-)} \rangle \langle \mathbf{k}^{(-)} \Phi_n | T^N | \Phi_i \mathbf{k}_i^{(+)} \rangle}{E^{(+)} - \varepsilon_k - \epsilon_n}. \quad (22)$$

To obtain the physical T matrix only the elastic term ($f = i$) requires modification due to the addition of the one-electron T matrix for the U_0 potential [9].

Using antisymmetry of the target states we may write the V-matrix elements of (17) as

$$\langle \mathbf{k}_f^{(-)} \Phi_f | V | \Phi_n \mathbf{k}^{(\pm)} \rangle = \langle \mathbf{k}_f^{(-)} \Phi_f | V_0 - U_0 + 2V_{01} | \Phi_n \mathbf{k}^{(\pm)} \rangle + 2\langle \mathbf{k}_f^{(-)} \Phi_f | (E - H_T - H_0 - V_{01} - V_{02}) P_{01} | \Phi_n \mathbf{k}^{(\pm)} \rangle. \quad (23)$$

The first term is the direct matrix element and the second term is the exchange matrix element.

We solve the coupled Lippmann-Schwinger equations for the T matrix by expanding (22) in partial waves J of the total orbital angular momentum, total spin S, and parity Π. The reduced V (or T) matrix elements are defined by

$$\langle L'k'^{(-)}(x_0), n'\pi'l's'(x_1, x_2) \parallel V_{\Pi S}^J \parallel Lk^{(\pm)}(x_0), n\pi ls(x_1, x_2) \rangle$$

$$= \sum_{\substack{M,m,\sigma,\nu \\ M',m',\sigma',\nu'}} C_{LlJ}^{MmM_J} C_{L'l'J}^{M'm'M_J} C_{\frac{1}{2}sS}^{\sigma\nu M_S} C_{\frac{1}{2}s'S}^{\sigma'\nu'M_S} \int d\hat{\mathbf{k}} \int d\hat{\mathbf{k}}' Y_{L'M'}^*(\hat{\mathbf{k}}') Y_{LM}(\hat{\mathbf{k}})$$

$$\times \langle \mathbf{k}'^{(-)}\sigma'(x_0) \Phi_{n'}^{\pi'l'm's'\nu'}(x_1, x_2) \mid V \mid \Phi_n^{\pi lms\nu}(x_1, x_2) \mathbf{k}^{(\pm)}\sigma(x_0) \rangle. \quad (24)$$

Here we use the coupled angular momentum form for the three-particle wave function

$$\mid Lk^{(\pm)}(x_0), n\pi ls(x_1, x_2) : JS\Pi \rangle$$

$$= (2/\pi)^{1/2}(kr_0)^{-1}i^L e^{\pm i\delta_L} u_L(kr_0) \sum_{\substack{\sigma,\nu \\ M,m}} C_{LlJ}^{MmM_J} C_{\frac{1}{2}sS}^{\sigma\nu M_S} Y_{LM}(\hat{\mathbf{r}}_0) \chi(\sigma) \Phi_n^{\pi lms\nu}(x_1, x_2), \quad (25)$$

where $u_L(kr_0)$ is the radial part [9] of the projectile wave function in partial wave J.

If the initial target state has $s = 0$ then the total spin takes only the value $S = 1/2$, otherwise $S = 3/2$ is also possible. For initial $l = 0$ states only the "natural" parity $\Pi = \pi(-1)^L = \pi'(-1)^{L'} = (-1)^J$ is used, otherwise the "unnatural" parity $\Pi = (-1)^{J+1}$ also arises.

Dropping the explicit space notation, the partial-wave Lippmann-Schwinger equation corresponding to (22) for the reduced T-matrix elements is

$$\langle L_f k_f^{(-)}, f\pi_f l_f s_f \| T_{\Pi S}^{JN} \| L_i k_i^{(+)}, i\pi_i l_i s_i \rangle$$

$$= \langle L_f k_f^{(-)}, f\pi_f l_f s_f \| V_{\Pi S}^J \| L_i k_i^{(+)}, i\pi_i l_i s_i \rangle$$

$$+ \sum_{n=1}^{N} \sum_{L} \sumint_{k} \frac{\langle L_f k_f^{(-)}, f\pi_f l_f s_f \| V_{\Pi S}^J \| Lk^{(-)}, n\pi ls \rangle \langle Lk^{(-)}, n\pi ls \| T_{\Pi S}^{JN} \| L_i k_i^{(+)}, i\pi_i l_i s_i \rangle}{E^{(+)} - \varepsilon_k - \epsilon_n}. \quad (26)$$

The method of solution of this equation is identical to the case of hydrogenic targets [9].

B. Numerical stability and uniqueness of the T matrix

The above derivation leads to formally correct coupled equations, but when solved numerically the required solutions may be unstable. This is due to the fact that the expansion (14) is too general, and does not define the scattering amplitudes f_n^N uniquely. For example, if we suppose that some functions g_n^N are such that

$$0 = (1 - P_{01} - P_{02}) \sum_{n=1}^{N} \Phi_n(x_1, x_2) g_n^N(x_0), \quad (27)$$

then it is clear that

$$\Psi^N(x_0, x_1, x_2) = (1 - P_{01} - P_{02})$$
$$\times \sum_{n=1}^{N} \Phi_n(x_1, x_2)[f_n^N(x_0) + \theta g_n^N(x_0)],$$
$$(28)$$

for any constant θ. This nonuniqueness of expansion manifests itself as numerical instability in the half-on-shell $T_{fi}(k, k_i)$ matrix. On the energy shell ($k = k_f$) Stelbovics [22] showed that the result should be unique due to the fact that the nonunique part of the T matrix is formally zero on the energy shell. However, computationally, on occasion we find that off-shell instability affects the on-shell results. This becomes evident when a small variation in the momentum quadrature grids leads to a large variation in the on-shell T-matrix elements [5].

This problem has been addressed for atomic hydrogen [1,22], and similarly for hydrogenic targets [9,10]. We first note that in order to satisfy (27) the functions g_n^N must be spanned by the same single-particle functions that are used in the CI expansion of the target states Φ_n. Therefore, we only need to address the problem of nonuniqueness in the expansion

$$I_0^N \psi^N(x_0, x_1, x_2) = \sum_{n=1}^{N} \Phi_n(x_1, x_2) I_0^N f_n^N(x_0), \quad (29)$$

where the projection operator I_0^N is made from the CI single-particle functions

$$I_0^N = \sum_{\alpha} |\varphi_\alpha\rangle\langle\varphi_\alpha|. \quad (30)$$

The nonuniqueness problem is solved by enforcing the condition that

$$P_{0i} \sum_{n=1}^{N} \Phi_n(x_1, x_2) I_0^N f_n(x_0)$$

$$= -\sum_{n=1}^{N} \Phi_n(x_1, x_2) I_0^N f_n(x_0), \quad i = 1, 2, \quad (31)$$

which ensures that $g_n^N = 0$ for any nonzero θ in (28). In other words, we specify that ψ^N is totally antisymmetric like Ψ^N, but only in the space spanned by the CI functions (see Ref. [10] for more detail). This condition is implemented numerically by considering the matrix element of the energy term in (19)

$$E\langle \mathbf{k}_f^{(-)}\Phi_f|P_{01}|\psi^N\rangle = (1 - \theta + \theta)E\langle \mathbf{k}_f^{(-)}\Phi_f|P_{01}I_0^N|\psi^N\rangle$$

$$= (1 - \theta)E\langle \mathbf{k}_f^{(-)}\Phi_f|P_{01}|\psi^N\rangle$$

$$- \theta E\langle \mathbf{k}_f^{(-)}\Phi_f|I_0^N|\psi^N\rangle, \quad (32)$$

which effectively imposes condition (31) for any nonzero constant θ. Whereas (32) introduces explicit θ and N dependence to the V-matrix elements the resultant T matrix remains unique on and off the energy shell. For some numerical examples, see Ref. [5]. More often than not even $\theta = 0$ gives the same on-shell T-matrix elements, but this is less reliable than for non-zero θ. Typically we take $\theta = 0.5$.

The symmetry condition (31) has the implicit assumption that such an expansion is possible. In the case where both electrons in Φ_n are treated equivalently this is the case. However, in the frozen-core approximation considerable care must be taken to impose antisymmetry in only the two-electron space of the projectile and a target electron whenever both electrons may be spanned by the same single-particle functions.

C. Calculation of the reduced V-matrix elements

We now use the CI representation of the helium target wave functions to express reduced V-matrix elements using the unsymmetrized functions (8), and write

$$\langle L'k'(x_0), n'\pi'l's'(x_1, x_2) \mid\mid V_{\Pi S}^J \mid\mid Lk(x_0), n\pi ls(x_1, x_2)\rangle$$

$$= \sum_{\alpha,\beta,\gamma,\delta} C_{\alpha\beta}^{(n')} C_{\gamma\delta}^{(n)} \langle L'k'(x_0), \varphi_\alpha(x_1)\varphi_\beta(x_2) : \pi'l's'||V_{\Pi S}^J||Lk(x_0), \varphi_\gamma(x_1)\varphi_\delta(x_2) : \pi ls\rangle. \quad (33)$$

Standard formulas of the tensor operator algebra [23] can be applied to calculate the matrix elements. From the structure of (26) it can be seen that the complex phases of (25) may be trivially factored out. For brevity of presentation we drop them from the following relations, and indicate when they should be restored.

1. Direct matrix elements

We use the multipole expansion of the potential in the direct matrix element, and write

$$V^D = V_0 - U_0 + 2V_{01}$$
$$\equiv 4\pi \sum_{\lambda,\mu} \frac{(-1)^\lambda}{2\lambda+1} v_\lambda(r_0,r_1) Y^*_{\lambda\mu}(\mathbf{r}_1) Y_{\lambda\mu}(\mathbf{r}_2), \qquad (34)$$

where

$$v_\lambda(r_0,r_1) = -\delta^\lambda_0 \delta(r_0 - r_1)\left(\frac{Z}{r_0} + U_0(r_0)\right) + 2\frac{r^\lambda_<}{r^{\lambda+1}_>}. \qquad (35)$$

Then the direct matrix element is given by

$$\langle L'k'(x_0), \varphi_\alpha(x_1)\varphi_\beta(x_2) : \pi'l's' || V^D || Lk(x_0), \varphi_\gamma(x_1)\varphi_\delta(x_2) : \pi ls\rangle$$

$$= \frac{2}{\pi k'k}\delta^s_{s'}\langle\varphi_\beta|\varphi_\delta\rangle\hat{l}\hat{l}'\hat{L}\hat{l}_\gamma \sum_\lambda (-1)^{l+l'+L+J+l_\alpha+l_\beta+\lambda} C^{000}_{L\lambda L'} C^{000}_{l_\gamma\lambda l_\alpha} \left\{\begin{matrix} l_\beta & l_\alpha & l' \\ \lambda & l & l_\gamma \end{matrix}\right\}\left\{\begin{matrix} L' & l' & J \\ l & L & \lambda \end{matrix}\right\}$$

$$\times \int dr_1 dr_0 u_L(kr_0) u_{L'}(k'r_0)\phi_\alpha(r_1)\phi_\gamma(r_1) v_\lambda(r_0,r_1), \qquad (36)$$

where we have used the shortened notation $\phi_\alpha \equiv \phi_{k_\alpha l_\alpha}$. The overlap integral between the single-particle functions is

$$\langle\varphi_\beta|\varphi_\delta\rangle = \delta^{l_\beta}_{l_\delta}\int dr \phi_\beta(r)\phi_\delta(r). \qquad (37)$$

The range of allowed values of λ is determined by triangle rules for angular momenta (l', λ, l), (L', λ, L), and $(l_\alpha, \lambda, l_\gamma)$.

2. Exchange matrix elements

Calculation of the exchange matrix elements involves the application of the corresponding space exchange op-

erator and consequently recoupling of the angular momenta to get the same coordinate ordering on the left and right sides of the matrix element. After this the calculation is a straightforward application of the tensor operator algebra relations.

We separate the exchange matrix element calculation into a number of steps. First we consider calculation of the matrix elements for the electron-electron potential V_{01}. To do this we apply the space exchange operator P_{01} to the right-hand side of the three-electron wave function and then recouple the angular momenta, resulting in

$$\langle L'k'(x_0), \varphi_\alpha(x_1)\varphi_\beta(x_2) : \pi'l's' || V_{01}P_{01} || Lk(x_0), \varphi_\gamma(x_1)\varphi_\delta(x_2) : \pi ls\rangle$$

$$= \frac{2}{\pi k'k}\langle\varphi_\beta|\varphi_\delta\rangle \sum_{j\lambda} (-1)^{l_\alpha+l_\beta+l_\gamma+l+l'+J+\lambda+1+s+s'}(2j+1)\hat{l}\hat{l}'\hat{s}\hat{s}'\hat{L}\hat{l}_\gamma C^{000}_{L\lambda l_\alpha} C^{000}_{l_\gamma\lambda L'}$$

$$\times \left\{\begin{matrix} L & l_\delta & j \\ l_\gamma & J & l \end{matrix}\right\}\left\{\begin{matrix} 1/2 & 1/2 & s' \\ 1/2 & S & s \end{matrix}\right\}\left\{\begin{matrix} l_\beta & l_\alpha & l' \\ \lambda & l & L \end{matrix}\right\}\left\{\begin{matrix} L' & l' & J \\ j & l_\gamma & \lambda \end{matrix}\right\}$$

$$\times \int dr_1 dr_0 u_L(kr_1) u_{L'}(k'r_0)\phi_\alpha(r_1)\phi_\gamma(r_0)\frac{r^\lambda_<}{r^{\lambda+1}_>}. \qquad (38)$$

We now turn to the electron-electron potential V_{02}. The space exchange operator P_{01} is applied to the right-hand side, but the angular momenta are recoupled for the three-electron wave function on the left-hand side, to obtain

$$\langle L'k'(x_0), \varphi_\alpha(x_1)\varphi_\beta(x_2) : \pi'l's' || V_{02}P_{01} || Lk(x_0), \varphi_\gamma(x_1)\varphi_\delta(x_2) : \pi ls\rangle$$

$$= \frac{2}{\pi k'k}(-1)^{L'+l'+l_\alpha+l_\beta+l_\gamma+1+s+s'}\hat{l}\hat{l}'\hat{s}\hat{s}'\hat{l}_\gamma\hat{l}_\delta\langle\varphi_\alpha|Lk\rangle$$

$$\times \sum_\lambda C^{000}_{l_\gamma\lambda L'} C^{000}_{l_\delta\lambda l_\beta} \left\{\begin{matrix} L' & l_\beta & l \\ l_\alpha & J & l' \end{matrix}\right\}\left\{\begin{matrix} L' & l_\beta & l \\ l_\delta & l_\gamma & \lambda \end{matrix}\right\}\left\{\begin{matrix} 1/2 & 1/2 & s \\ 1/2 & S & s' \end{matrix}\right\}$$

$$\times \int dr_0 dr_2 \frac{r^\lambda_<}{r^{\lambda+1}_>} u_{L'}(k'r_0)\phi_\beta(r_2)\phi_\gamma(r_0)\phi_\delta(r_2). \qquad (39)$$

The overlap integral between the projectile wave function and the one-electron orbital is

$$\langle\varphi_\alpha|Lk\rangle = \delta_L^{l_\alpha} \int dr\phi_\alpha(r)u_L(kr). \tag{40}$$

Calculation of the matrix elements of the target Hamiltonian (1) has to be done explicitly because the relation $H_T\Phi_n = \epsilon_n\Phi_n$ holds only for true eigenstates. We first consider the calculation of the matrix elements for the two-electron potential V_{12}. Here it is convenient to recouple the angular momenta on the right-hand side, to obtain

$$\langle L'k'(x_0), \varphi_\alpha(x_1)\varphi_\beta(x_2) : \pi'l's'||V_{12}P_{01}||Lk(x_0), \varphi_\gamma(x_1)\varphi_\delta(x_2) : \pi ls\rangle$$

$$= \frac{2}{\pi k'k}(-1)^{L'+l'+l_\alpha+l_\beta+l_\gamma+1+s+s'}\hat{l}\hat{l'}\hat{s}\hat{s'}\hat{L}\hat{l}_\delta\langle\varphi_\gamma|L'k'\rangle\sum_\lambda C_{L\lambda l_\alpha}^{000}C_{l_\delta\lambda l_\beta}^{000}\begin{Bmatrix}L & l_\delta & l' \\ l_\gamma & J & l\end{Bmatrix}\begin{Bmatrix}L & l_\delta & l' \\ l_\beta & l_\gamma & \lambda\end{Bmatrix}\begin{Bmatrix}1/2 & 1/2 & s \\ 1/2 & S & s'\end{Bmatrix}$$

$$\times \int dr_1 dr_2 \frac{r_<^\lambda}{r_>^{\lambda+1}}u_L(kr_1)\phi_\alpha(r_1)\phi_\beta(r_2)\phi_\delta(r_2). \tag{41}$$

The remaining operators of H_T are H_1 and H_2. These may be combined with the H_0 term to yield

$$\langle L'k'(x_0), \varphi_\alpha(x_1)\varphi_\beta(x_2) : \pi'l's'||(E - H_0 - H_1 - H_2)P_{01}||Lk(x_0), \varphi_\gamma(x_1)\varphi_\delta(x_2) : \pi ls\rangle$$

$$= \frac{2}{\pi k'k}\Bigg((-1)^{L+l+l'+l_\gamma+1+s+s'}\hat{l}\hat{l'}\hat{s}\hat{s'}\begin{Bmatrix}L & l_\delta & l' \\ l_\gamma & J & l\end{Bmatrix}\begin{Bmatrix}1/2 & 1/2 & s \\ 1/2 & S & s'\end{Bmatrix}$$

$$\times\Bigg[\langle\varphi_\alpha|Lk\rangle\langle\varphi_\beta|\varphi_\delta\rangle\langle L'k'|\varphi_\gamma\rangle[E(1-\theta) - \varepsilon_{k'} - \varepsilon_k]$$

$$-\langle\varphi_\alpha|Lk\rangle\langle\varphi_\beta|\varphi_\delta\rangle\langle L'k'|V_0 - U_0|\varphi_\gamma\rangle - \langle L'k'|\varphi_\gamma\rangle\langle\varphi_\beta|\varphi_\delta\rangle\langle\varphi_\alpha|V_1 - U_1|Lk\rangle$$

$$-\langle L'k'|\varphi_\gamma\rangle\langle\varphi_\alpha|Lk\rangle\langle\varphi_\beta|H_2|\varphi_\delta\rangle\Bigg] - E\theta\langle L'k'|I_0^N|Lk\rangle\langle\varphi_\beta|\varphi_\delta\rangle\langle\varphi_\alpha|\varphi_\gamma\rangle\Bigg), \tag{42}$$

where we have used (20) and (32). The overlap integral between the projectile wave function, the one-electron potential, and the one-electron orbital is, for example,

$$\langle\varphi_\alpha|V_1|Lk\rangle = -Z\delta_L^{l_\alpha}\int dr\phi_\alpha(r)u_L(kr)/r. \tag{43}$$

The matrix element of H_2 contains K_2 which is handled using analytical properties of the Laguerre functions.

For the higher partial waves J the two-electron exchange matrix elements (39) and (41) and one-electron exchange matrix elements (42) disappear due to the overlap integrals between the one-electron orbitals and the projectile wave functions.

If the calculated target wave functions are good approximations to the exact target eigenfunctions then the relation $H_T\Phi_n = \epsilon_n\Phi_n$ can be used to simplify calculation of the exchange matrix elements. Using the relation

$$H_0 + V_{02} = H_T(x_0, x_2) - H_2 \tag{44}$$

for true eigenstates $n'l's'$ and nls we obtain

$$\langle L'k'(x_0), n'l's'(x_1, x_2) || [H_T(x_1, x_2) + V_{02} + H_0]P_{01} || Lk(x_0), nls(x_1, x_2)\rangle$$

$$= \langle L'k'(x_0), n'l's'(x_1, x_2) || (\epsilon_{n'} + \epsilon_n - H_2)P_{01} || Lk(x_0), nls(x_1, x_2)\rangle, \tag{45}$$

which is much simpler to calculate.

In summary, the full reduced matrix element for a particular J, S, and Π is the sum of (36), (38), (39), (41), and (42), multiplied by the appropriate complex phase factors in (25). Note that the above relations for the reduced matrix elements do not make the assumption of the frozen-core model.

IV. RESULTS

In this work it is our aim to demonstrate that the CCC method is able to provide a relatively accurate description of electron-helium scattering, irrespective of projectile energy or transition of interest. Thus far we have presented the CCC formalism for the electron-helium scattering problem assuming nonrelativistic quantum mechanics, and that the center of mass is at the nucleus. As is the case with the CCC method for the atomic hydrogen target no further assumptions are introduced. However, in the latter case we only need to establish convergence in the one-electron target space, whereas in the former the target space contains two-electron excitation. Using desk-top computational resources we have no way of treating the full two-electron target space. Instead, we introduce the approximation of treating the helium target

by the frozen-core model (FCM), where we restrict one of the electrons to be the $1s$ He^+ orbital. The FCM approximation reduces convergence studies to treating only one-electron excitation. Our tests of this approximation for low energy elastic scattering, which requires very few expansion states, showed negligible effect.

To fulfill our aim we shall demonstrate good agreement with experiment at a broad range of energies, and a large number of transitions. This is a rather substantial task which involves the testing of convergence at each projectile energy. To simplify convergence studies, in the most difficult intermediate energy region, we present at most three calculations, denoted by CCC(75), CCC(69), and CCC(63). The former has a maximum of 169 channels and couples a total of 75 states consisting of 12 ^1S, 11 each of ^3S, ^1P, and ^3P, nine each of ^1D and ^3D, and six each of ^1F and ^3F states. The 69-state calculation has a maximum of 133 channels, and couples 13 ^1S, 12 each of ^3S, ^1P, and ^3P, and ten each of ^1D and ^3D states. The last couples 63 states consisting of 12 ^1S, 11 each of ^3S, ^1P, and ^3P, and nine each of ^1D and ^3D, with a maximum of 121 coupled channels. Note that a state with orbital angular momentum l generates a maximum of $l + 1$

channels. For this reason inclusion of higher target-state l leads to a rapid growth in the size of the calculation. Thus the CCC(75) calculation has the largest $l_{max} = 3$, but the CCC(69) calculation has more states within each l for $0 \leq l \leq l_{max} = 2$. The difference between the two calculations gives a good indication of the accuracy of convergence within the frozen-core model. In the case where the CCC(75) and the CCC(69) results are a little different the CCC(63) may be used to suggest which of the calculations is likely to be more accurate. The difference between the CCC(75) and CCC(63) results is solely due to the addition of 12 F states in the former. The difference between CCC(69) and CCC(63) results is solely due to the increase, by one for each target symmetry, of the Laguerre basis sizes. The two larger calculations are close to the limit of our desk-top workstation computational resources.

In this work we have chosen to give a broad overview of the CCC method for electron-helium scattering. For this reason we shall not concentrate on presenting detailed discussion of each figure. Instead, for the sake of brevity, we shall make only brief comments and rely on the interested reader to obtain the detailed information from the figures and tabular entries.

A. Differential cross sections

We begin the presentation of differential cross sections by starting with low energy elastic cross sections. These
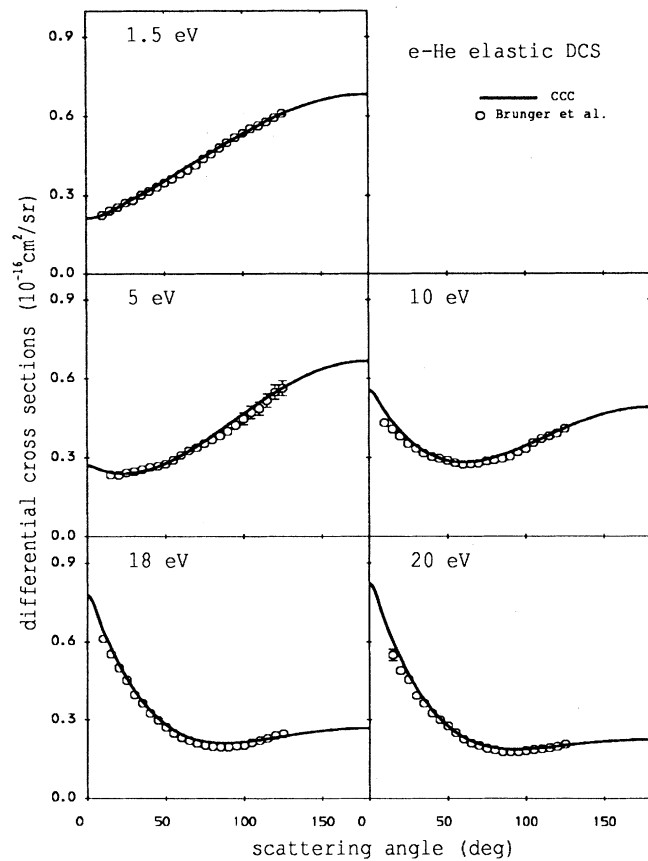

FIG. 1. Elastic differential cross sections for e-He scattering at a range of projectile energies. The present calculations are denoted by CCC, and are described in the text. The measurements are due to Brunger et $al.$ [12]. Quantitative results may be obtained from the authors.
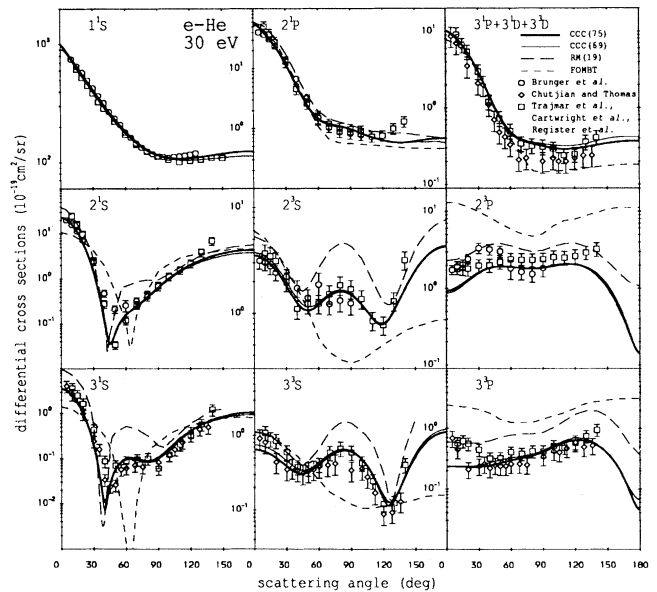

FIG. 2. Differential cross sections for e-He scattering at a projectile energy of 30 eV. The present calculations are denoted by CCC(75) and CCC(69), and are described in the text. The calculations denoted by RM(19) are due to Fon, Berrington, and Kingston [39], and those denoted by FOMBT are due to Cartwright et $al.$ [40] and Trajmar et $al.$ [25]. The measurements are due to Brunger et $al.$ [41], Brunger et $al.$ [12] (elastic), Trajmar et $al.$ [25], Cartwright et $al.$ [40] (n ^1P, $3D$), Register, Trajmar, and Srivastava [30] (elastic), and Chutjian and Thomas [42].

are particularly simple to obtain at the low energies as very few states are required. The experimental and theoretical situation here is very well understood, and has been for quite some time; see Ref. [12], for example. Thus we present CCC results here purely for completeness. They are given in Fig. 1, where convergence is readily established by using as few as ten states at 1.5 eV and 41 states at 20 eV, and agreement with experiment is very good. As the FCM approximation is most severe for the $1\,^1S$ state, see Table I, good agreement with experiment here is most encouraging.

One of the more extensively studied projectile energies is that of 30 eV (we treat data at 29.6 eV as though they were for 30 eV). Here there are measurements from various groups for excitation up to $n \leq 3$ levels. There are also a number of other theories, none of which can claim agreement with all of the available differential cross sections. Our CCC results together with some of the available measurements and theories are presented in Fig. 2. The first point to note is the negligible difference between the CCC(75) and CCC(69) calculations. Agreement with experiment is very good, and is much superior to the other theories presented. Given the demonstrated level of convergence it is interesting to note the minor discrepancy with the independent sets of measurements at the forward angles of the $n\,^3P$ channels. This could well be due to a systematic numerical problem that affects both

calculations, or due to the frozen-core approximation, or difficulties associated with measuring electrons scattered to forward angles. Overall we are satisfied that the CCC theory is adequate for describing the presented experimental differential cross sections at 30 eV.

In Fig. 3 we look at similar differential cross sections for the projectile energy of 40 eV. Conclusions are much the same as for the 30 eV results. Discrepancy with experiment at the forward angles for the triplet channels is a little more evident, but once again overall agreement of both the CCC(75) and CCC(69) theories with experiment is satisfactory. This quality of agreement with experiment is only possible if the helium target one-electron continuum is treated. For quantitative difference between CCC and CC calculations which do, and do not, treat the continuum at this energy see Ref. [24].

The 50 eV results are presented in Fig. 4. Here agreement with the experiment of Trajmar et al. [25] is at first glance worse than at the two lower energies. However, we note that our theory is systematically lower than their measurements, which are obtained as a ratio to the $2\,^1P$ channel. Thus, if we were to use the theoretical $2\,^1P$ differential cross section, instead of the experimental one, for generating the other differential cross sections we would find considerably improved agreement with experiment. Support for our results is also provided by the much earlier measurements of Hall et al. [26]. It is worthwhile noting that, unlike for the 30 and 40 eV results, agreement at the forward angles with the measurements of triplet states is very good.
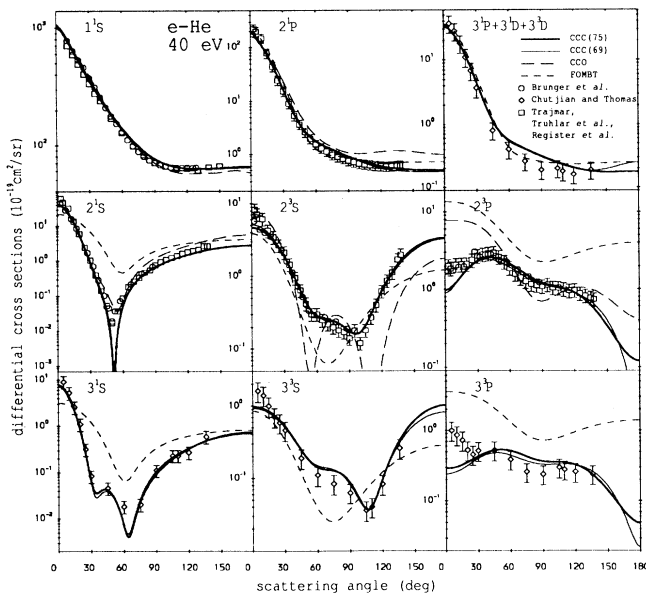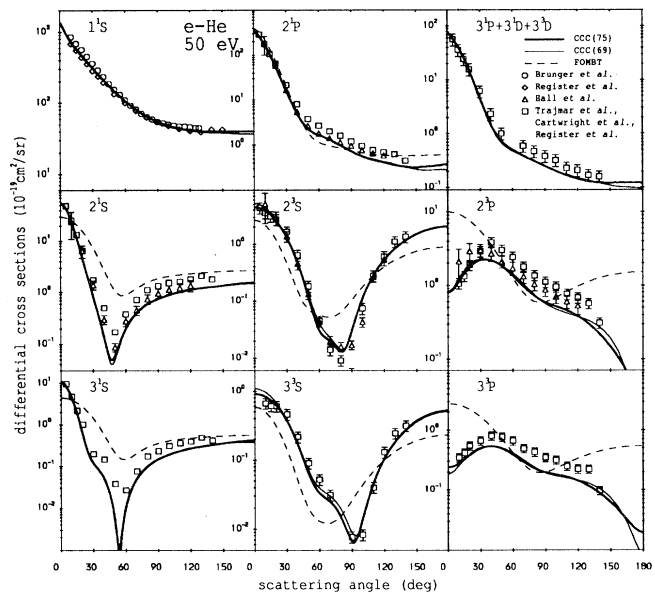

FIG. 3. Differential cross sections for e-He scattering at a projectile energy of 40 eV. The present calculations are denoted by CCC(75) and CCC(69), and are described in the text. The calculations denoted by CCO are due to McCarthy, Ratnavelu, and Zhou [11] and those denoted by FOMBT are due to Cartwright et al. [40] and Trajmar et al. [25]. The measurements are due to Brunger et al. [12] (elastic), Brunger et al. [41] (ratio measurements multiplied by our theoretical $2\,^1P$), Trajmar [43] ($2\,^1S, 2\,^3S, 2\,^3P$), Register, Trajmar, and Srivastava [30] (elastic), Truhlar et al. [44] ($2\,^1P$), and Chutjian and Thomas [42].

FIG. 4. Differential cross sections for e-He scattering at a projectile energy of 50 eV. The present calculations are denoted by CCC(75) and CCC(69), and are described in the text. The calculations denoted by FOMBT are due to Cartwright et al. [40] and Trajmar et al. [25]. The measurements are due to Brunger et al. [12], Register, Trajmar, and Srivastava [30], Trajmar et al. [25], Cartwright et al. [40] ($n\,^1P, 3D$), and Hall et al. [26].

In Fig. 5 we present differential cross sections for 80 eV incident projectile energy. Here there are no measurements of the cross sections for excitation of the $n = 3$ states, but we present these results for completeness. Agreement with experiment for the elastic and the $n = 2$ states is very good. Discrepancy with other theories is still substantial, though the FOMBT has considerably improved the description of the $2\,^3S$ and $2\,^3P$ states. Examining the difference between the two CCC calculations suggests that slightly larger calculations are necessary to get better accuracy.

At 100 eV, presented in Fig. 6, we are once more able to compare with measurements for all of the $n \le 3$ states. The difficulties at 50 eV are not apparent here, since agreement with experiment is excellent for all presented cross sections. This suggests that our 50 eV results are equally reliable. Convergence in the CCC calculations is very good at all but the very large angles. It is interesting to note that for the triplet channels the CCC theory is now above the measurements at the forward angles.

We next look at differential cross sections for 200 eV electron-impact excitation of helium. These are given in Fig. 7. Once more convergence is very good, and both the CCC(75) and CCC(69) results are in excellent agreement with available experiment. We note one exception to this at the very forward angles for the $2\,^3S$ excitation, where

the CCC theory is considerably below the measurements of Yoshinari et al. [27]. Anomalous forward angle measurements have been found in the same group earlier by Sakai et al. [28]. We are unable to confirm these results. Agreement with the forward angle measurements by this group of the $2\,^1P$ transition is excellent.

A similar result is also observed at 500 eV, shown in Fig. 8. Here there are nearly three orders of magnitude difference between theory and the experiment of Yoshinari et al. [27] near zero degrees. However, agreement with the same group's measurements for the $2\,^1P$ excitation remains excellent.

B. Integrated cross sections

Having presented differential cross sections we now discuss the corresponding integrated cross sections. In addition, we also give the total ionization σ_i and total σ_t cross sections. The latter is obtained either by the use of the optical theorem or by summing the cross sections for all open states included in the CC formalism. The former is obtained by summing only those cross sections which correspond to states with positive energies. These cross sections together with their partial target-state l contributions are given in Fig. 9, and are found to be in very good agreement with experiment. The results from the CCC(69) calculations are presented because for these
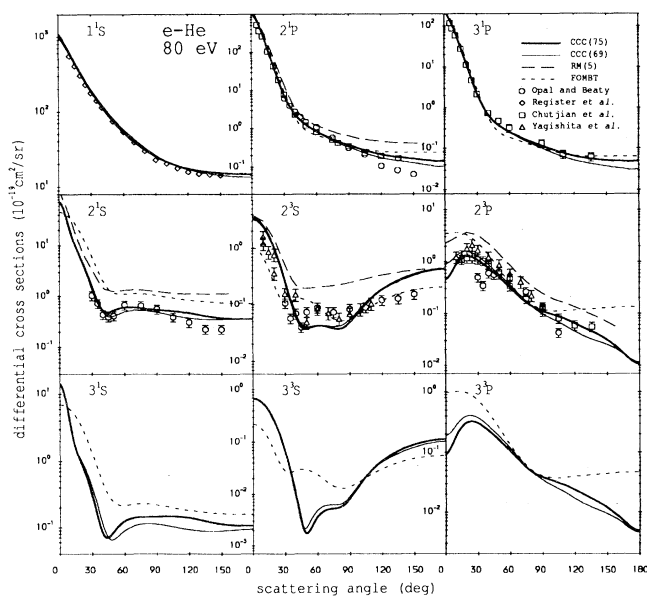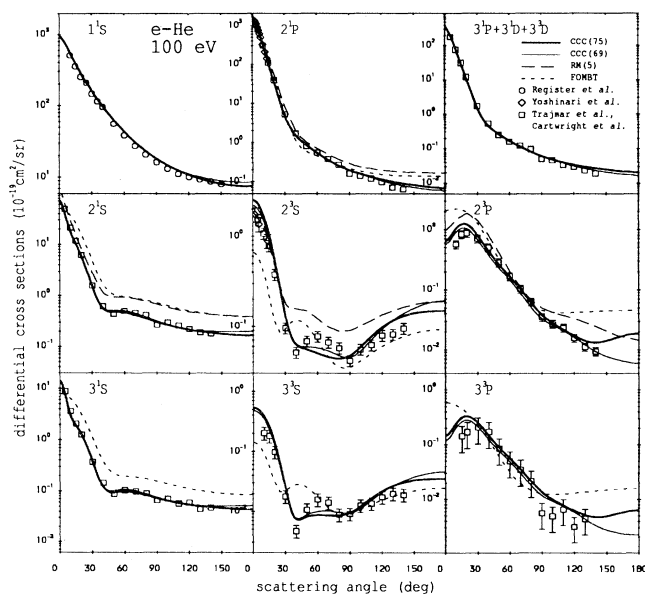

FIG. 5. Differential cross sections for e-He scattering at a projectile energy of 80 eV. The present calculations are denoted by CCC(75) and CCC(69), and are described in the text. The calculations denoted by RM(5) are due to Fon, Berrington, and Kingston [45] and Fon et al. [46], and those denoted by FOMBT are due to Cartwright et al. [40] and Trajmar et al. [25]. The measurements are due to Register, Trajmar, and Srivastava [30], Chutjian and Srivastava [47] ($2\,^1P$, $2\,^3P$), and Chutjian [48] ($3\,^1P$) (renormalized using the more accurate elastic differential cross section (DCS) of Register, Trajmar, and Srivastava), Opal and Beaty [49], and Yagishita, Takayanagi, and Suzuki [50].

FIG. 6. Differential cross sections for e-He scattering at a projectile energy of 100 eV. The present calculations are denoted by CCC(75) and CCC(69), and are described in the text. The calculations denoted by RM(5) are due to Fon, Berrington, and Kingston [45] and Fon et al. [46], and those denoted by FOMBT are due to Cartwright et al. [40] and Trajmar et al. [25]. The measurements are due to Register, Trajmar, and Srivastava [30], Cartwright et al. [40], Trajmar et al. [25], and Yoshinari et al. [27].
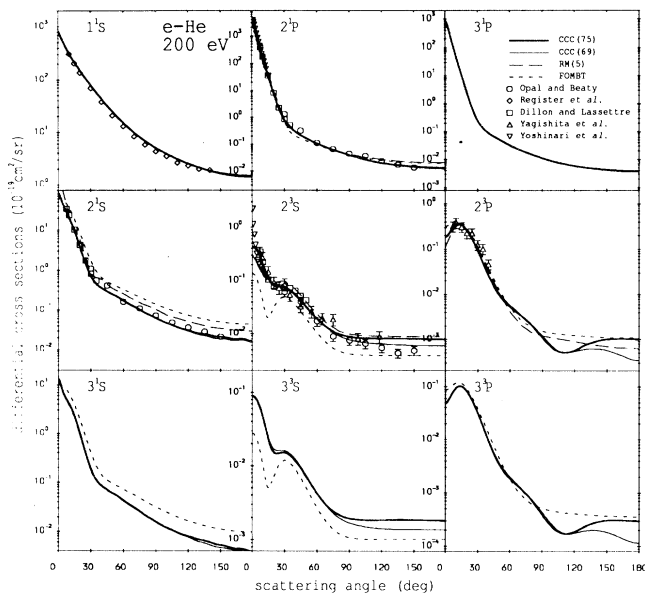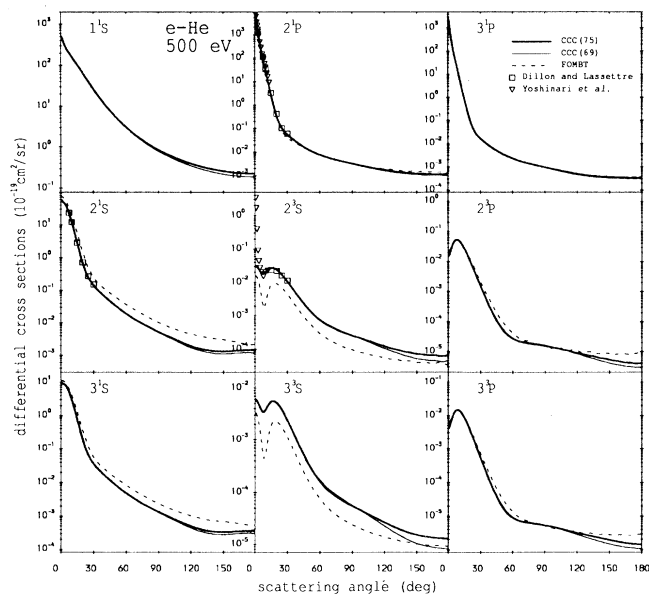
FIG. 7. Differential cross sections for e-He scattering at a projectile energy of 200 eV. The present calculations are denoted by CCC(75) and CCC(69), and are described in the text. The calculations denoted by RM(5) are due to Fon, Berrington, and Kingston [45] and Fon *et al.* [46], and those denoted by FOMBT are due to Cartwright *et al.* [40], and Trajmar *et al.* [25]. The measurements are due to Register, Trajmar, and Srivastava [30], Opal and Beaty [49], Yagishita, Takayanagi, and Suzuki [50], Yoshinari *et al.* [27], Dillon and Lassettre [51] $(2\,^1S, 2\,^1P)$, and Dillon [52] $(2\,^3S)$.

FIG. 8. Differential cross sections for e-He scattering at a projectile energy of 500 eV. The present calculations are denoted by CCC(75) and CCC(69), and are described in the text. The calculations denoted by FOMBT are due to Cartwright *et al.* [40] and Trajmar *et al.* [25]. The measurements are due to Yoshinari *et al.* [27], Dillon and Lassettre [51] $(2\,^1S, 2\,^1P)$, and Dillon [52] $(2\,^3S)$.
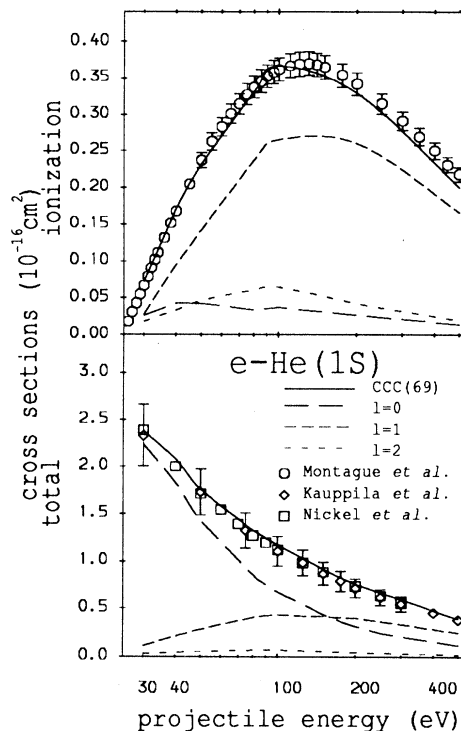

FIG. 9. Total ionization and total cross sections for electron-impact excitation of the ground state of helium. The solid line is the summed contribution of the s, p, and d individual contributions. The measurements are due to Montague, Harrison, and Smith [35], Kauppila *et al.* [37], and Nickel *et al.* [36].

transitions we believe them to be the most accurate (see below).

As the integrated cross sections are very important in practical applications, we give a more detailed convergence study here than for the differential cross sections. It is important to note that we shall attempt to demonstrate convergence within the frozen-core model. We have no formal way of estimating the magnitude of the error of this approximation. Good agreement with angular dependent measurements suggests to us that generally this error will not often exceed 10%. Apart from presenting the 75- and 69-state results, we also give the 63-state results. These calculations and some corresponding measurements are presented in Table II.

The rate of convergence varies with both transition of interest and the projectile energy. The purpose of presenting the 63-state results is to give an indication as to which of the 75- or 69-state results is likely to be more accurate in case they significantly differ. Suppose that for a particular transition and energy the 63- and 75-state results are similar, but the 69-state results are a little different, e.g., σ_i at 80 eV. This suggests that for this case the F states give little contribution, and so it is the 69-state results that are likely to be the most accurate. On the other hand, if the 69-state and the 63-state results are similar, but the 75-state results are a little different, e.g., $3\,^1D$ at all energies, then it is likely that the F

states make a significant contribution and so the latter should be more accurate. If both the 75- and 69-state results are different from the 63-state results, then both F states and higher basis sizes are necessary for greater accuracy. In this case taking the average of the three calculations may be appropriate. Variations between the three calculations can be viewed as error estimates on the frozen-core model results. It may be that in some cases the difference between the true and the frozen-core model results is greater than that between the three CCC calculations.

Upon examination of Table II we see generally good agreement with available measurements, though on occasion there are significant discrepancies. Most encour-

aging is the excellent agreement at all energies with the measurements of σ_i and σ_t, where the error bars are very small. The ability to obtain the total ionization cross section validates the discretization of the continuum via the Laguerre basis. The quality of agreement with experiment here is of the same order as for the hydrogen [7] and He$^+$ [29] targets. Because of the unitarity of the CC formalism, simply obtaining the correct σ_i at a particular energy gives us great confidence in the accuracy of all other transitions at this same energy.

The elastic cross section measurements of Register, Trajmar, and Srivastava [30] also claim small errors, but appear to be systematically a little lower than the CCC results for the higher energies. However, for energies

TABLE II. Integrated cross sections (cm^2) for electrons scattering on the ground state of helium at a range of energies (eV). The ionization and total cross sections are denoted by σ_i and σ_t, respectively. Square brackets denote powers of ten. The experimental estimates are due to Montague, Harrison, and Smith [35] (ionization, 4.5% error), Nickel et al. [36] (total, 1% error), Kauppila et al. [37] (total at 500 eV, 14% error), Register, Trajmar, and Srivastava [30] (elastic, 5% error), and de Heer et al. [38] (compilation of excitation cross sections, $n\,^1S$, $n\,^1P$: 10% error; $3\,^1D$ 20% error; triplet states: 30% error 100 eV and below, uncertain above 100 eV).

State	Calculation or experiment	30	40	50	80	100	200	500
$1\,^1S$	CCC(75)	2.25[-16]	1.69[-16]	1.34[-16]	7.59[-17]	6.22[-17]	2.76[-17]	9.88[-18]
	CCC(69)	2.16[-16]	1.74[-16]	1.35[-16]	7.99[-17]	6.19[-17]	2.73[-17]	9.83[-18]
	CCC(63)	2.25[-16]	1.68[-16]	1.34[-16]	7.60[-17]	6.18[-17]	2.76[-17]	9.86[-18]
	expt.	2.11[-16]	1.58[-16]	1.26[-16]	7.12[-17]	5.61[-17]	2.47[-17]	
$2\,^3S$	CCC(75)	1.91[-18]	1.14[-18]	7.32[-19]	2.56[-19]	1.53[-19]	2.82[-20]	2.62[-21]
	CCC(69)	1.96[-18]	1.13[-18]	7.53[-19]	2.45[-19]	1.50[-19]	2.79[-20]	2.58[-21]
	CCC(63)	1.93[-18]	1.16[-18]	7.33[-19]	2.46[-19]	1.52[-19]	2.83[-20]	2.62[-21]
	expt.	1.90[-18]	1.18[-18]	7.40[-19]	2.60[-19]	1.40[-19]	2.40[-20]	2.49[-21]
$2\,^1S$	CCC(75)	2.19[-18]	1.87[-18]	1.67[-18]	1.37[-18]	1.16[-18]	7.98[-19]	3.89[-19]
	CCC(69)	2.06[-18]	1.86[-18]	1.67[-18]	1.27[-18]	1.11[-18]	7.94[-19]	3.88[-19]
	CCC(63)	2.20[-18]	1.89[-18]	1.66[-18]	1.33[-18]	1.14[-18]	7.93[-19]	3.87[-19]
	expt.	2.40[-18]	2.11[-18]	1.94[-18]	1.50[-18]	1.30[-18]	8.38[-19]	4.24[-19]
$2\,^3P$	CCC(75)	2.19[-18]	1.71[-18]	1.07[-18]	3.29[-19]	2.14[-19]	2.62[-20]	1.45[-21]
	CCC(69)	2.19[-18]	1.63[-18]	1.11[-18]	3.70[-19]	1.82[-19]	2.60[-20]	1.44[-21]
	CCC(63)	2.19[-18]	1.72[-18]	1.10[-18]	3.53[-19]	2.20[-19]	2.62[-20]	1.44[-21]
	expt.	2.60[-18]	1.90[-18]	1.40[-18]	4.91[-19]	2.80[-19]	3.60[-20]	1.90[-21]
$2\,^1P$	CCC(75)	3.86[-18]	6.59[-18]	8.18[-18]	1.06[-17]	1.10[-17]	9.05[-18]	5.50[-18]
	CCC(69)	3.78[-18]	6.58[-18]	8.36[-18]	1.10[-17]	1.11[-17]	9.10[-18]	5.55[-18]
	CCC(63)	3.81[-18]	6.66[-18]	8.33[-18]	1.09[-17]	1.12[-17]	9.10[-18]	5.52[-18]
	expt.	3.75[-18]	6.43[-18]	8.21[-18]	1.01[-17]	1.01[-17]	8.32[-18]	5.67[-18]
$3\,^3S$	CCC(75)	5.39[-19]	3.15[-19]	1.83[-19]	5.75[-20]	3.34[-20]	6.04[-21]	5.58[-22]
	CCC(69)	5.71[-19]	3.03[-19]	1.94[-19]	5.52[-20]	3.28[-20]	5.94[-21]	5.50[-22]
	CCC(63)	5.38[-19]	3.11[-19]	1.89[-19]	5.49[-20]	3.32[-20]	6.04[-21]	5.58[-22]
	expt.	6.58[-19]	4.91[-19]	2.61[-19]	7.90[-20]	4.20[-20]	7.18[-21]	7.49[-22]
$3\,^1S$	CCC(75)	4.37[-19]	3.64[-19]	3.30[-19]	2.89[-19]	2.37[-19]	1.69[-19]	8.71[-20]
	CCC(69)	4.37[-19]	3.78[-19]	3.36[-19]	2.58[-19]	2.30[-19]	1.69[-19]	8.69[-20]
	CCC(63)	4.35[-19]	3.76[-19]	3.34[-19]	2.79[-19]	2.35[-19]	1.68[-19]	8.68[-20]
	expt.	3.91[-19]	3.95[-19]	3.38[-19]	2.62[-19]	2.33[-19]	1.46[-19]	8.45[-20]
$3\,^3P$	CCC(75)	5.07[-19]	4.61[-19]	3.10[-19]	1.00[-19]	6.59[-20]	8.23[-21]	4.50[-22]
	CCC(69)	5.41[-19]	4.26[-19]	3.18[-19]	1.12[-19]	5.57[-20]	8.13[-21]	4.49[-22]
	CCC(63)	5.01[-19]	4.57[-19]	3.10[-19]	1.06[-19]	6.78[-20]	8.24[-21]	4.49[-22]
	expt.	7.38[-19]	5.30[-19]	3.83[-19]	1.42[-19]	8.15[-20]	1.02[-20]	5.29[-22]
$3\,^3D$	CCC(75)	1.08[-19]	6.07[-20]	3.57[-20]	7.78[-21]	4.13[-21]	3.26[-22]	1.30[-23]
	CCC(69)	1.24[-19]	8.02[-20]	4.38[-20]	9.95[-21]	4.18[-21]	3.19[-22]	1.29[-23]
	CCC(63)	1.25[-19]	7.44[-20]	4.51[-20]	8.79[-21]	4.45[-21]	3.18[-22]	1.30[-23]
	expt.	1.70[-19]	9.82[-20]	5.10[-20]	1.53[-20]	1.00[-20]	1.60[-21]	4.55[-22]
$3\,^1D$	CCC(75)	2.06[-19]	2.28[-19]	2.18[-19]	1.73[-19]	1.45[-19]	7.55[-20]	2.67[-20]
	CCC(69)	2.26[-19]	2.82[-19]	2.64[-19]	1.97[-19]	1.56[-19]	7.62[-20]	2.69[-20]
	CCC(63)	2.33[-19]	2.85[-19]	2.63[-19]	1.96[-19]	1.56[-19]	7.58[-20]	2.69[-20]
	expt.	2.28[-19]	2.59[-19]	2.61[-19]	1.86[-19]	1.44[-19]	7.06[-20]	2.42[-20]
$3\,^1P$	CCC(75)	7.26[-19]	1.40[-18]	1.88[-18]	2.46[-18]	2.62[-18]	2.23[-18]	1.37[-18]
	CCC(69)	7.34[-19]	1.36[-18]	1.90[-18]	2.55[-18]	2.64[-18]	2.24[-18]	1.38[-18]
	CCC(63)	7.22[-19]	1.37[-18]	1.89[-18]	2.54[-18]	2.66[-18]	2.24[-18]	1.37[-18]
	expt.	7.38[-20]	1.38[-18]	1.84[-18]	2.42[-18]	2.44[-18]	2.08[-18]	1.29[-18]
σ_i	CCC(75)	6.48[-18]	1.62[-17]	2.39[-17]	3.59[-17]	3.63[-17]	3.27[-17]	1.96[-17]
	CCC(69)	7.18[-18]	1.72[-17]	2.32[-17]	3.32[-17]	3.67[-17]	3.29[-17]	2.00[-17]
	CCC(63)	6.44[-18]	1.62[-17]	2.37[-17]	3.57[-17]	3.59[-17]	3.25[-17]	1.95[-17]
	expt.	6.70[-18]	1.68[-17]	2.37[-17]	3.38[-17]	3.62[-17]	3.42[-17]	2.18[-17]
σ_t	CCC(75)	2.47[-16]	2.03[-16]	1.76[-16]	1.31[-16]	1.18[-16]	7.57[-17]	3.86[-17]
	CCC(69)	2.39[-16]	2.08[-16]	1.76[-16]	1.33[-16]	1.18[-16]	7.53[-17]	3.88[-17]
	CCC(63)	2.47[-16]	2.02[-16]	1.76[-16]	1.31[-16]	1.17[-16]	7.55[-17]	3.85[-17]
	expt.	2.39[-16]	2.00[-16]	1.72[-16]	1.27[-16]	1.12[-16]	7.34[-17]	3.82[-17]

ranging between 1.5 and 50 eV the CCC results are in excellent agreement with the measurements of Brunger *et al.* [12] (see the differential cross section figures), and so we suggest that the presented CCC results are within 10% of the true elastic integrated cross sections at all energies.

We have not presented the cross sections for states with $n \geq 4$ because of the insufficiently large bases used. Access to more substantial computational facilities than those available to us would be necessary for obtaining accurate cross sections for such excitations.

C. Electron-impact coherence parameters

A considerably stronger test of the calculated scattering amplitudes is provided by comparison with measurements of the electron-impact coherence parameters (EICP's). These describe the charge cloud after excitation. For a comprehensive review of this subject see Ref. [18]. For excitation of nP states the EICP's $L_\perp$, γ, and P_ℓ, together with the differential cross section, are sufficient to test the magnitudes and phases of the scattering amplitudes. Many measurements of P-state EICP's have been performed for electron-impact excitation of helium at a broad range of energies, allowing for the most complete test of our theory to date. In practice the EICP's are not directly measured, but rather are derived from angular correlation or polarization correlation measurements. The various relations between scattering amplitudes and experimentally measured quantities may be found in Ref. [18].

In the case of excitation of nD states the scattering amplitudes have six independent real numbers to be tested at each scattering angle. An additional EICP ρ_{00} may be experimentally obtained. Though the four measured EICP's are all that are available for testing theory, the complexity of these transitions is sufficient to provide a stringent, if not complete, test of the scattering theory. It is also customary to present the total polarization P parameter, but this is not independent of the other four.

It may be helpful to emphasize that, since the CCC theory is based on the close-coupling formalism, a single calculation for a particular projectile energy results simultaneously in scattering amplitudes for each of the states included. This may be contrasted with distorted-wave approximations, where a separate calculation is performed for each transition of interest. Therefore it is more convenient to look at the CCC results separately for each projectile energy.

1. EICP's at 30 eV for e-He excitation

We start by presenting in Fig. 10 the results for the $2\,^1P$ EICP's at 30 eV. Comparison of the two CCC theories shows excellent convergence and they are in good agreement with experiment as is the 19-state R-matrix calculation. The FOMBT is very different, indicating that this energy is too low for a first-order Born-based approximation to be accurate. The fact that the R-matrix
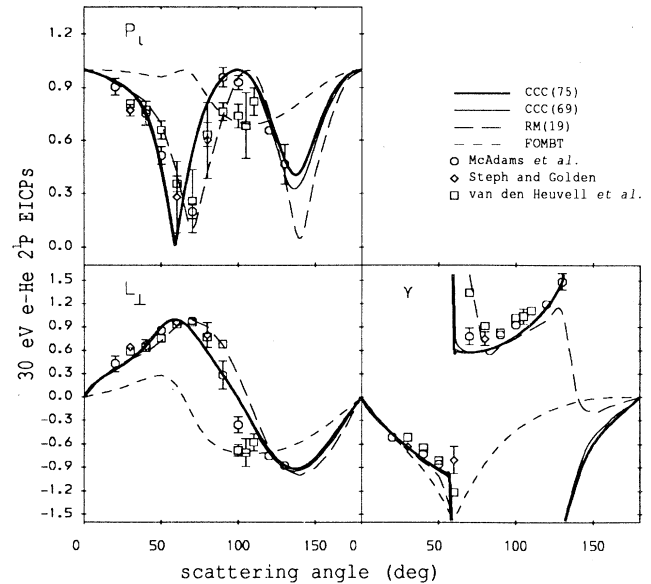

FIG. 10. The $2\,^1P$ EICP's for 30 eV e-He scattering. The present calculations are denoted by CCC(75) and CCC(69), and are described in the text. The calculations denoted by RM(19) are due to Fon, Berrington, and Kingston [39], and those denoted by FOMBT are due to Cartwright *et al.* [40]. The measurements are due to McAdams *et al.* [53], Steph and Golden [54], and van den Heuvell, van Eck, and Heideman [55].

calculation gets such good agreement with experiment suggests that for this transition the treatment of the target continuum is not very important.

The $3\,^1P$ EICP's are presented in Fig. 11. Here we see that, though the CCC(75) and CCC(69) are very similar, the latter are in slightly better agreement with experiment indicating that the effect of a larger Laguerre basis size within each symmetry is a little more important than the inclusion of F states. The R-matrix calculation has more difficulty in describing the experiment here than for the $2\,^1P$ transition.

In Fig. 12 we present EICP's for the exchange transition $3\,^3P$. Here the conclusions are much the same as for the $3\,^1P$ excitation. Convergence of the CCC calculations and agreement with experiment is satisfactory, with the R-matrix calculation being only marginally worse than the CCC theory. The FOMBT is equally inappropriate for exchange transitions at these relatively low energies.

Having completed our presentation of EICP's for P-state excitation we turn to the EICP's for $3\,^1D$ excitation. In Fig. 13 we present not only the EICP's but also the directly measured Stokes parameters from which the EICP's are derived [18]. We do this simply to indicate that sometimes the derived parameters may be very sensitive and that discrepancy with theory in this case is not cause for alarm. If we concentrate on the independent measurements of P_1, P_2, P_3, and P_4 we see that convergence in the CCC theory is quite good and agreement with experiment is satisfactory, in contrast to the DWBA calculations. Yet when we look at the γ =ATAN2
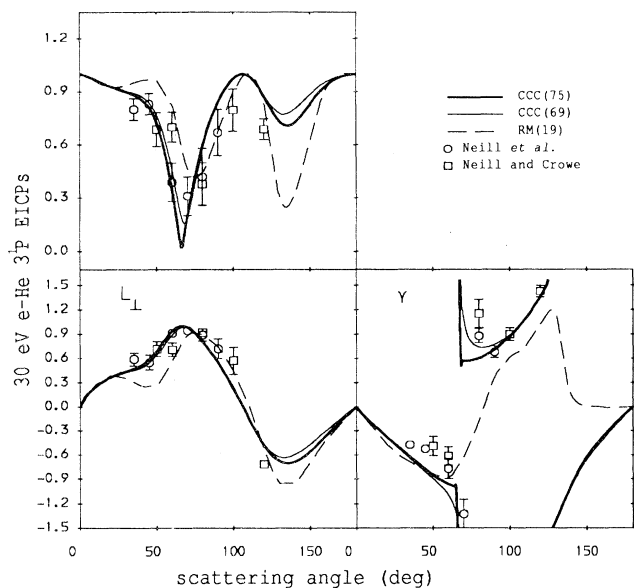
FIG. 11. The $3\,^1P$ EICP's for 30 eV e-He scattering. The present calculations are denoted by CCC(75) and CCC(69), and are described in the text. The calculations denoted by RM(19) are due to Fon, Berrington, and Kingston [39]. The measurements are due to Neill and Crowe [56], and Neill, Donnelly, and Crowe [57].
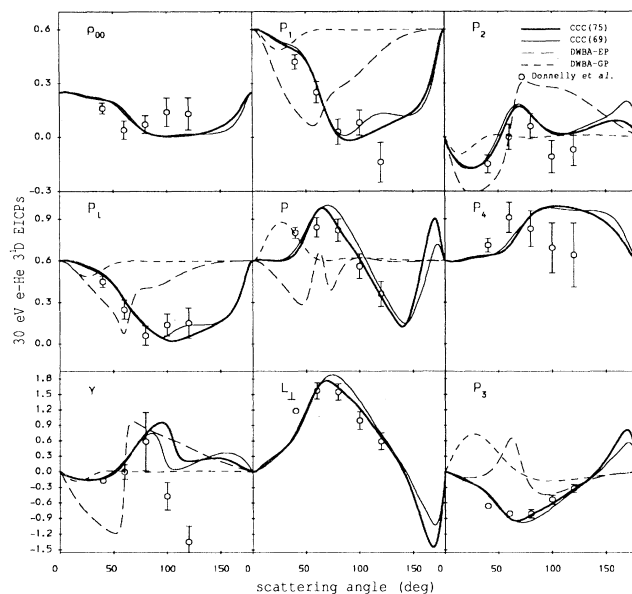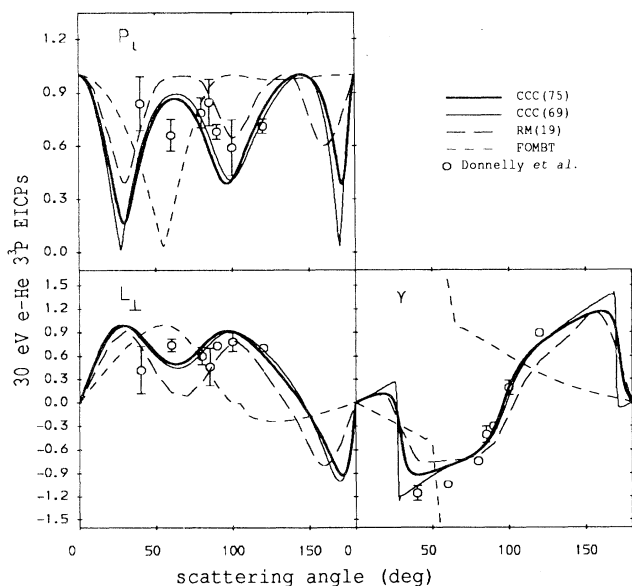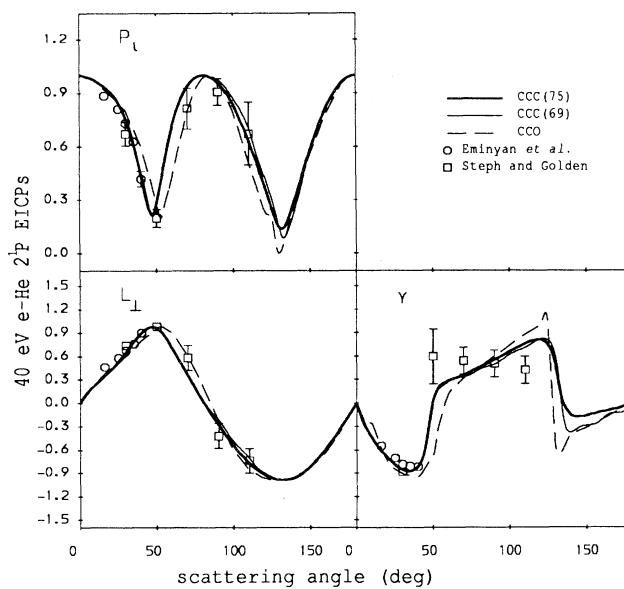
FIG. 13. The $3\,^1D$ EICP's for 30 eV e-He scattering. The present calculations are denoted by CCC(75) and CCC(69), and are described in the text. The calculations denoted by DWBA-EP and DWBA-GP are due to Bartschat and Madison [16]. The measurements are due to Donnelly, McLaughlin, and Crowe [60].

FIG. 12. The $3\,^3P$ EICP's for 30 eV e-He scattering. The present calculations are denoted by CCC(75) and CCC(69), and are described in the text. The calculations denoted by RM(19) are due to Fon, Berrington, and Kingston [39], and those denoted by FOMBT are due to Cartwright and Csanak [58]. The measurements are due to Donnelly, Neill, and Crowe [59].
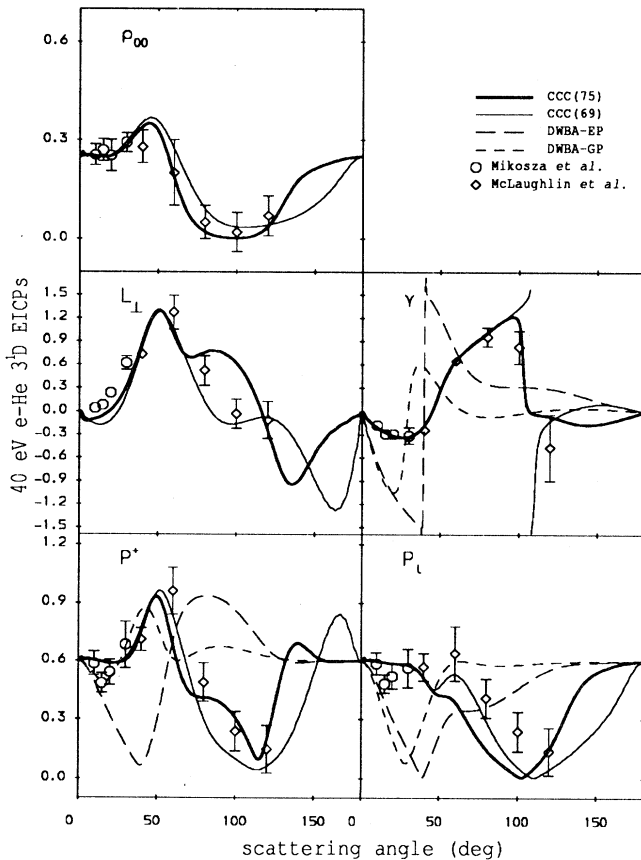
FIG. 14. The $2\,^1P$ EICP's for 40 eV e-He scattering. The present calculations are denoted by CCC(75) and CCC(69), and are described in the text. The calculations denoted by CCO are due to McCarthy, Ratnavelu, and Zhou [11]. The measurements are due to Eminyan et $al.$ [61] and Steph and Golden [54].

$(P_1, P_2)/2$ parameter (where ATAN2 is the FORTRAN function) agreement between theory and experiment looks particularly poor. This sensitivity is due to the fact that both P_1 and P_2 are near zero at the backward angles.

2. EICP's at 40 eV for e-He excitation

At 40 eV there are only extensive measurements for the $2\,^1P$, $3\,^1D$, and $3\,^3D$ excitations. The former are presented in Fig. 14 and are compared with the CCC and CCO results. Once more convergence has been established and agreement of all theories and experiment is satisfactory.

In Fig. 15 we present the EICP's for the $3\,^1D$ excitation. Here we note that convergence is not quite to the same accuracy as we have noted before, indicating the difficulty of the calculation. However, there is clear qualitative agreement of both CCC calculations with experiment, in marked contrast to the DWBA theory. As both of the CCC calculations are at the limit of our desktop computational resources, we are unable to refine the

FIG. 16. The $3\,^3D$ EICP's for 40 eV e-He scattering. The present calculations are denoted by CCC(75) and CCC(69), and are described in the text. The calculations denoted by DWBA-EP and DWBA-GP are due to Bartschat and Madison [16]. The measurements are due to Crowe et al. [31], Batelaan, van Eck, and Heideman [64], and Beyer, Silim, and Kleinpoppen [65].

CCC results further. The integrated results given in Table II suggest that the 75-state results are likely to be the most accurate in this case. Given that we are looking at a D-state excitation one would expect that inclusion of F states in the CC formalism should have some effect.

The $3\,^3D$ excitation EICP's and the corresponding directly measured Stokes parameters are given in Fig. 16. The relation between the Stokes parameters, their reduced counterparts, and the EICP's may be found in Ref. [31]. Here it is helpful to present the Stokes parameters because some experimental groups have measured only a subset of these, which does not allow them to be related to the EICP's. As for the $3\,^1D$ EICP's convergence has not been established to a high accuracy, indicating the difficulty of this calculation. The CCC(75) calculation is in better agreement with experiment, which suggests that inclusion of F states for the description of the $3\,^3D$ excitation is also important.

3. EICP's at 50 eV for e-He excitation

The EICP's for the $2\,^1P$ excitation at 50 eV are presented in Fig. 17. Convergence in the CCC calculations is quite good as is the agreement with experiment. The DWBA gives a good reproduction of the experiment at forward angles, but goes wrong at intermediate and backward angles.

Similar conclusions are also appropriate for the $3\,^1P$ EICP's, presented in Fig. 18. It is interesting to note the

FIG. 15. The $3\,^1D$ EICP's for 40 eV e-He scattering. The present calculations are denoted by CCC(75) and CCC(69), and are described in the text. The calculations denoted by DWBA-EP and DWBA-GP are due to Bartschat and Madison [16]. The measurements are due to McLaughlin, Donnelly, and Crowe [62] and Mikosza et al. [63].
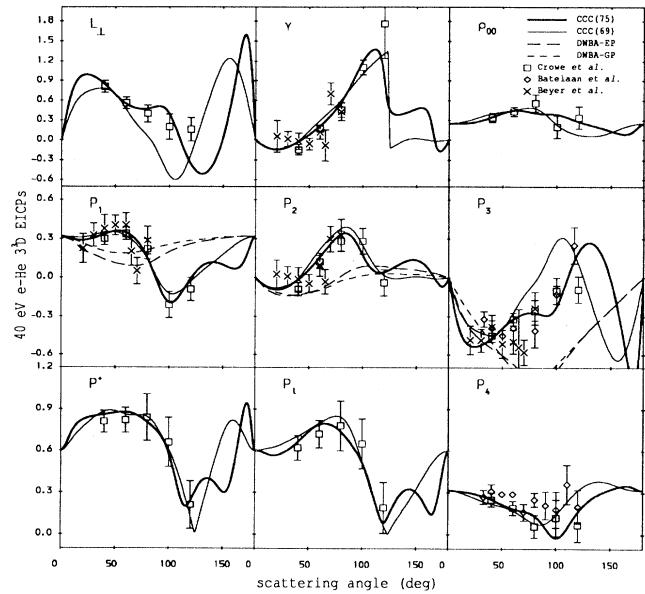
excellent agreement for the γ parameter, suggesting that the experimental difficulty evident at intermediate angles for $L_\perp$ and P_ℓ did not affect the ratio of P_2 to P_1.

4. EICP's at 80 eV for e-He excitation

In Fig. 19 we give the EICP's for the $2\,^1P$ excitation at 80 eV. From the P_ℓ and γ parameters it is evident that the 75-state calculation is marginally superior to the 69-state one. The CCC calculations are in very good agreement with all of the measurements other than those due to Steph and Golden [32]. Prior to application of the CCC theory the previous R-matrix and DWBA theories were unable to conclusively demonstrate which of the measurements were likely to be more accurate.

The $3\,^1P$ EICP's are given in Fig. 20. Once more it is interesting to note how well the γ parameter is described by the CCC theory. Yet agreement with $P_\ell = \sqrt{P_1^2 + P_2^2}$ is not as good at the intermediate angles. Given the established convergence we suspect that this is primarily due to experimental difficulties.

5. EICP's at 100 eV for e-He excitation

There are no large angle measurements of the $2\,^1P$ EICP's at 100 eV, presented in Fig. 21. This is because the cross section gets to be very small at these angles (see Fig. 6). For the CCC theory higher energies are particularly easy to calculate, due to the the ease of the solution of the integral equations (26). From the figure it is clear
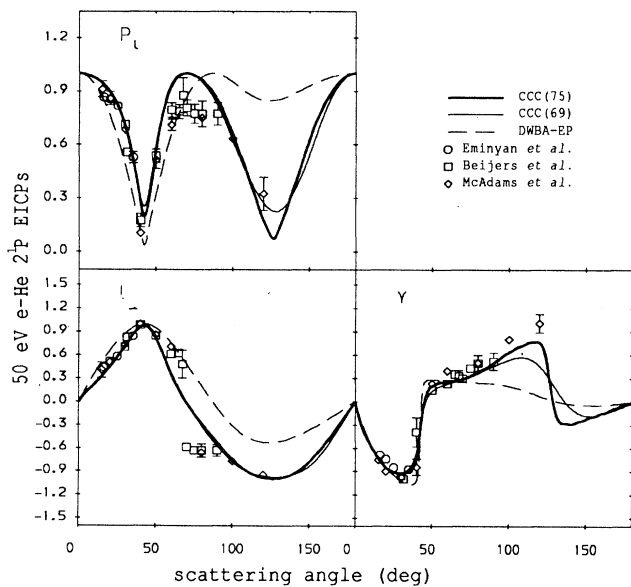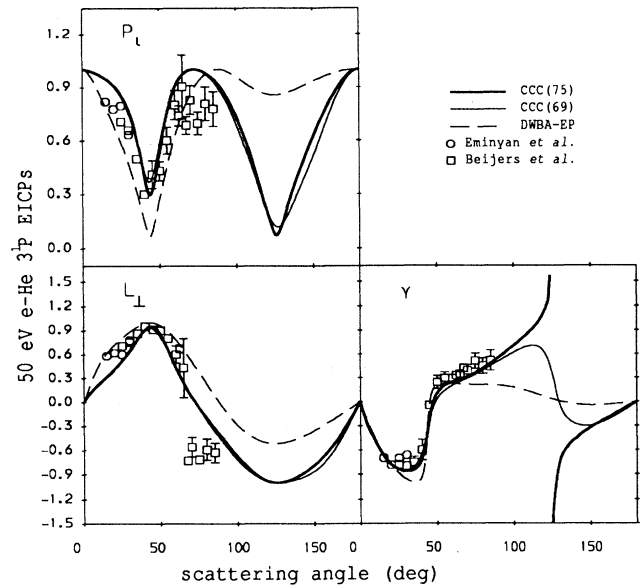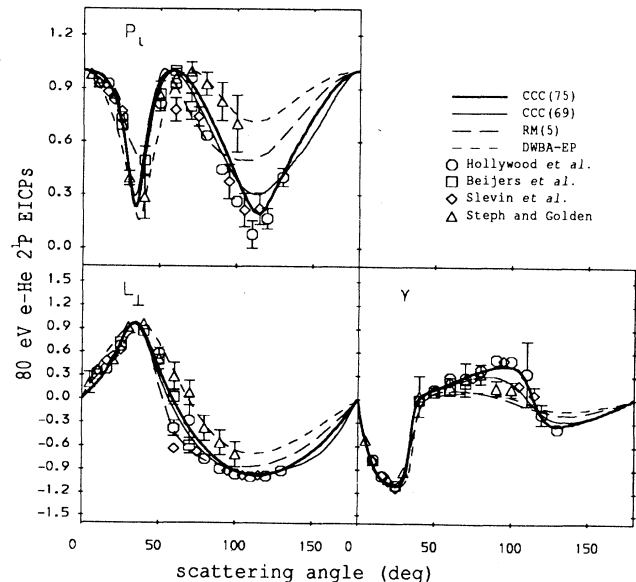

FIG. 18. The $3\,^1P$ EICP's for 50 eV e-He scattering. The present calculations are denoted by CCC(75) and CCC(69), and are described in the text. The calculations denoted by DWBA-EP are due to Beijers $et\ al.$ [66]. The measurements are due to Eminyan $et\ al.$ [67] and Beijers $et\ al.$ [66].

FIG. 17. The $2\,^1P$ EICP's for 50 eV e-He scattering. The present calculations are denoted by CCC(75) and CCC(69), and are described in the text. The calculations denoted by DWBA-EP are due to Beijers $et\ al.$ [66]. The measurements are due to Eminyan $et\ al.$ [61], McAdams $et\ al.$ [53], and Beijers $et\ al.$ [66].

FIG. 19. The $2\,^1P$ EICP's for 80 eV e-He scattering. The present calculations are denoted by CCC(75) and CCC(69), and are described in the text. The calculations denoted by DWBA-EP are due to Beijers $et\ al.$ [66] and those denoted by RM(5) are due to Fon, Berrington, and Kingston [45]. The measurements are due to Hollywood, Crowe, and Williams [68], Beijers $et\ al.$ [66], Slevin $et\ al.$ [69], and Steph and Golden [32].
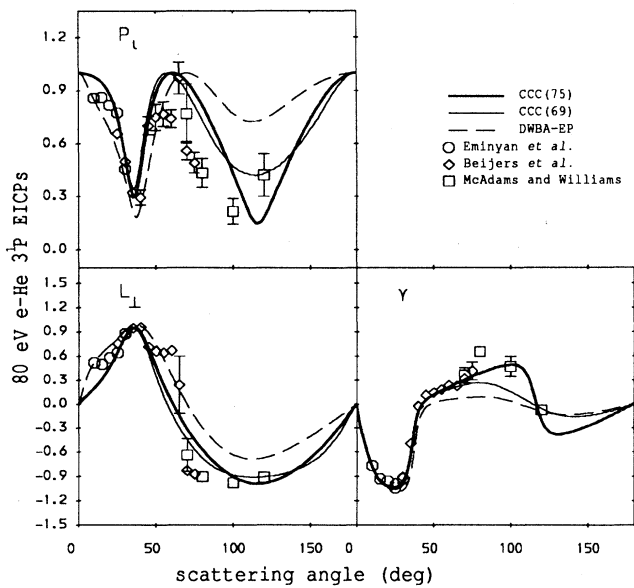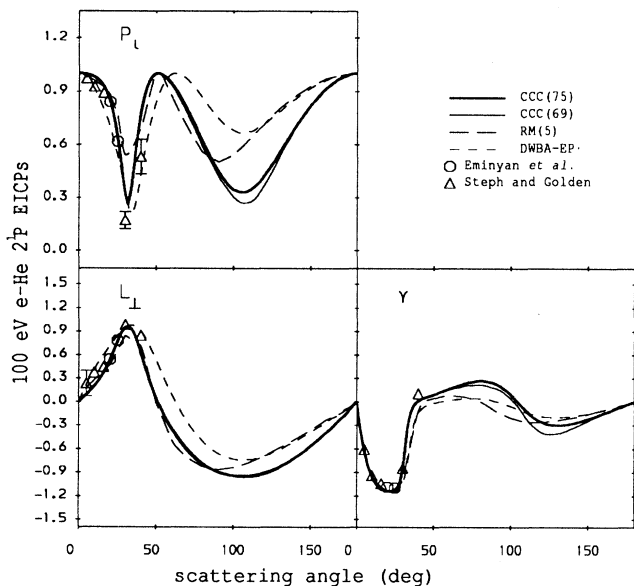
FIG. 20. The $3\,^1P$ EICP's for 80 eV e-He scattering. The present calculations are denoted by CCC(75) and CCC(69), and are described in the text. The calculations denoted by DWBA-EP are due to Beijers $et\ al.$ [66]. The measurements are due to Eminyan $et\ al.$ [67], Beijers $et\ al.$ [66], and McAdams and Williams [70].

that convergence has been established, and the results are in good agreement with experiment. The five-state R-matrix calculation is unable to obtain the first deep minimum of the P_ℓ parameter, whereas the DWBA does.

The $3\,^1P$ EICP's for 100 eV incident electrons are given in Fig. 22. Once more convergence is readily established, agreement with the available experiment being excellent. Though agreement between the CCC and DWBA theories is very good at forward angles, the former systematically obtains a lower minimum for the P_ℓ parameter.

6. $2\,^1P$ EICP's at 200 and 500 eV for e-He excitation

The 200 and 500 eV $2\,^1P$ EICP's are given in Figs. 23 and 24, respectively. The two CCC calculations are barely distinguishable, and are in good agreement with experiment, which is only available at forward angles.

V. CONCLUSIONS

We have demonstrated that the CCC method for the calculation of electron-helium scattering is able to obtain qualitative, and often quantitative, agreement with measurements of differential, integrated, ionization, and total cross sections, as well as various EICP's for $n \le 3$ states, for projectile energies ranging from 1.5 to 500 eV. As such it is the only scattering theory that is able to achieve this to date. This gives us further confidence that the long-standing discrepancy with the electron-hydrogen EICP's at 54.4 eV [1] is primarily due to experiment. As we have
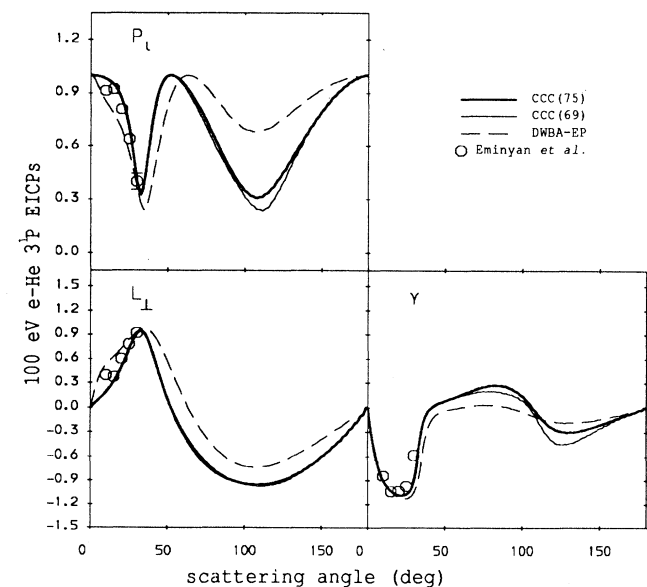

FIG. 21. The $2\,^1P$ EICP's for 100 eV e-He scattering. The present calculations are denoted by CCC(75) and CCC(69), and are described in the text. The calculations denoted by DWBA-EP are due to Beijers $et\ al.$ [66] and those denoted by RM(5) are due to Fon, Berrington, and Kingston [45]. The measurements are due to Eminyan $et\ al.$ [61] and Steph and Golden [32].

FIG. 22. The $3\,^1P$ EICP's for 100 eV e-He scattering. The present calculations are denoted by CCC(75) and CCC(69), and are described in the text. The calculations denoted by DWBA-EP are due to Madison [71]. The measurements are due to Eminyan $et\ al.$ [67].
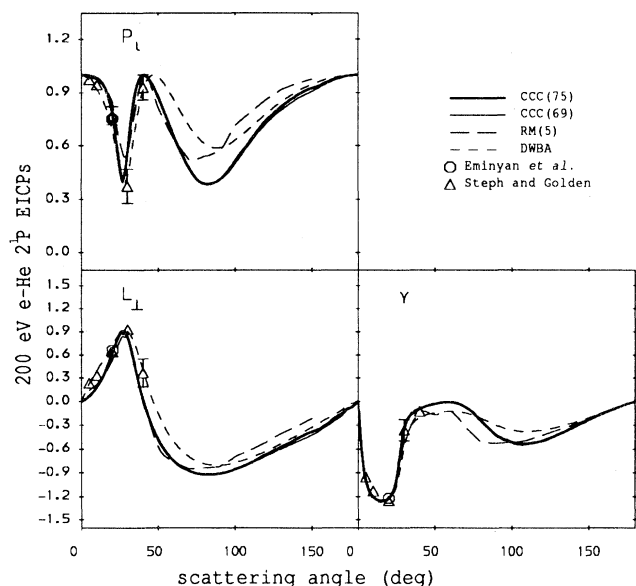
FIG. 23. The $2\,^1P$ EICP's for 200 eV e-He scattering. The present calculations are denoted by CCC(75) and CCC(69), and are described in the text. The calculations denoted by DWBA-EP are due to Madison [71] and those denoted by RM(5) are due to Fon, Berrington, and Kingston [45]. The measurements are due to Eminyan et al. [61] and Steph and Golden [32].

FIG. 24. The $2\,^1P$ EICP's for 500 eV e-He scattering. The present calculations are denoted by CCC(75) and CCC(69), and are described in the text. The measurements are due to Steph and Golden [32].

found earlier for the sodium target [9], once reasonable accuracy in the target wave functions is obtained, it becomes more important to treat accurately the scattering part of the calculation.

By using the frozen-core approximation we have not attempted to give the most accurate results possible, but rather to give a general overview of the quality of our scattering techniques. The CCC method has been implemented to include full two-electron excitation, and so we may readily improve the target-state energies by introducing extra configurations. However, in this case we generate a great many more states than what we can hope to include in the close-coupling formalism using our desktop computational facilities. For this reason we have only presented the results from the frozen-core model. Should it be demonstrated that practical applications require greater than the given accuracy then we would require more substantial computational resources. If we concentrate only on the elastic channel, then by dropping F and maybe most D states, we can probably provide more accurate elastic cross sections, still using our local computational facilities. More accurate treatment of
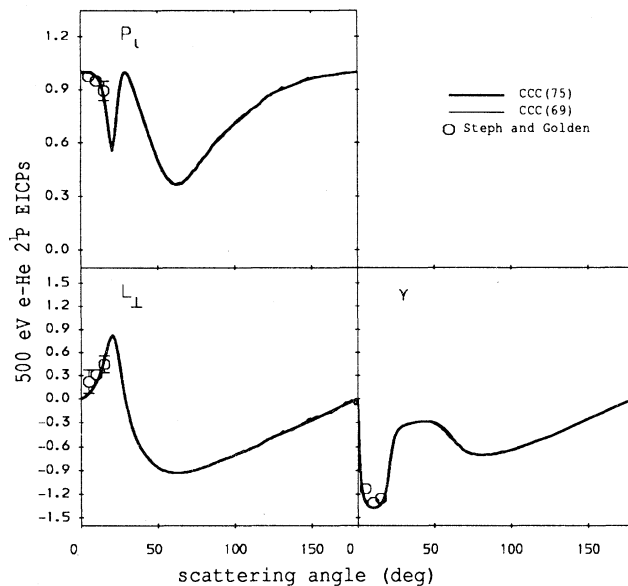
the helium target would also be necessary for studies of threshold and resonance behavior of cross sections. We note, however, that Fon, Lim, and Sawey [33] have calculated resonances using structure approximations which are a little worse than the frozen-core approximation.

The computational implementation of the electron-helium scattering problem has been done on top of the code developed for hydrogenic targets [9]. Thus the current CCC computer code may now be readily extended to treat heliumlike atoms and ions. We also expect to apply the CCC method to the calculation of scattering from the $2\,^{1,3}S$ helium states, as well as differential $(e, 2e)$ cross sections.

ACKNOWLEDGMENTS

[1] I. Bray and A. T. Stelbovics, Phys. Rev. A **46**, 6995 (1992).

[2] A. Temkin, Phys. Rev. **126**, 130 (1962).

[3] R. Poet, J. Phys. B **11**, 3081 (1978).

[4] I. Bray and A. T. Stelbovics, Phys. Rev. Lett. **69**, 53

(1992).

[5] I. Bray and A. T. Stelbovics, Comput. Phys. Commun. **85**, 1 (1995).

[6] I. Bray and A. T. Stelbovics, At. Data Nucl. Data Tables **58**, 67 (1994).

[7] I. Bray and A. T. Stelbovics, Phys. Rev. Lett. **70**, 746 (1993).

[8] I. Bray, D. A. Konovalov, I. E. McCarthy, and A. T. Stelbovics, Phys. Rev. A **50**, R2818 (1994).

[9] I. Bray, Phys. Rev. A **49**, 1066 (1994).

[10] I. Bray and A. T. Stelbovics, Adv. At. Mol. Phys. **35**, 209 (1995).

[11] I. E. McCarthy, K. Ratnavelu, and Y. Zhou, J. Phys. B **23**, 1325 (1990).

[12] M. J. Brunger et al., J. Phys. B **25**, 1823 (1992).

[13] W. C. Fon, K. A. Berrington, and A. Hibbert, J. Phys. B **14**, 307 (1981).

[14] W. C. Fon, K. P. Lim, K. Ratnavelu, and P. M. J. Sawey, J. Phys. B **27**, 1561 (1994).

[15] W. C. Fon, K. P. Lim, and K. A. Berrington, J. Phys. B **27**, L591 (1994).

[16] K. Bartschat and D. H. Madison, J. Phys. B **21**, 153 (1988).

[17] D. C. Cartwright and G. Csanak, J. Phys. B **20**, L583 (1987).

[18] N. Andersen, J. W. Gallagher, and I. V. Hertel, Phys. Rep. **165**, 1 (1988).

[19] K. A. Berrington and A. E. Kingston, J. Phys. B **20**, 6631 (1987).

[20] M. Cohen and P. S. Kelly, Can. J. Phys. **45**, 2079 (1967).

[21] S. Cameron, R. P. McEachran, and M. Cohen, Can. J. Phys. **48**, 211 (1970).

[22] A. T. Stelbovics, Phys. Rev. A **41**, 2536 (1990).

[23] D. A. Varshalovich, *Quantum Theory of Angular Momentum*, 1st ed. (World Scientific, Philadelphia, 1988).

[24] I. Bray, D. V. Fursa, and I. E. McCarthy, Phys. Rev. A **51**, 500 (1995).

[25] S. Trajmar, D. F. Register, D. C. Cartwright, and G. Csanak, J. Phys. B **25**, 4889 (1992).

[26] R. I. Hall et al., J. Phys. (Paris) **34**, 827 (1973).

[27] Y. Yoshinari et al., in *XVII International Conference on the Physics of Electronic and Atomic Collisons, Abstracts*, edited by W. R. MacGillivray, I. E. McCarthy, and M. C. Standage (Griffith University, Brisbane, 1991), p. 139.

[28] Y. Sakai et al., Phys. Rev. A **43**, 1656 (1991).

[29] I. Bray, I. E. McCarthy, J. Wigley, and A. T. Stelbovics, J. Phys. B **26**, L831 (1993).

[30] D. F. Register, S. Trajmar, and S. K. Srivastava, Phys. Rev. A **21**, 1134 (1980).

[31] A. Crowe et al., J. Phys. B **27**, L795 (1994).

[32] N. C. Steph and D. E. Golden, Phys. Rev. A **21**, 1848 (1980).

[33] W. C. Fon, K. L. Lim, and P. M. J. Sawey, J. Phys. B **26**, 305 (1993).

[34] C. E. Moore, *Atomic Energy Levels*, Natl. Bur. Stand. (U.S.) Circ. No. 467 (U.S. GPO, Washington, DC, 1949), Vol. 1.

[35] R. G. Montague, M. F. A. Harrison, and A. C. H. Smith, J. Phys. B **17**, 3295 (1984).

[36] J. C. Nickel, K. Imre, D. F. Register, and S. Trajmar, J. Phys. B **18**, 125 (1985).

[37] W. E. Kauppila et al., Phys. Rev. A **24**, 725 (1981).

[38] F. J. de Heer, R. Hoekstra, A. E. Kingston, and H. P. Summers, Nucl. Fusion Suppl. **3**, 19 (1992).

[39] W. C. Fon, K. A. Berrington, and A. E. Kingston, J. Phys. B **24**, 2161 (1991).

[40] D. C. Cartwright, G. Csanak, S. Trajmar, and D. F. Register, Phys. Rev. A **45**, 1602 (1992).

[41] M. J. Brunger et al., J. Phys. B **23**, 1325 (1990).

[42] A. Chutjian and L. D. Thomas, Phys. Rev. A **11**, 1583 (1975).

[43] S. Trajmar, Phys. Rev. A **8**, 191 (1973).

[44] D. G. Truhlar et al., Phys. Rev. A **8**, 2475 (1973).

[45] W. C. Fon, K. A. Berrington, and A. E. Kingston, J. Phys. B **13**, 2309 (1980).

[46] W. C. Fon, K. A. Berrington, and A. E. Kingston, J. Phys. B **12**, 1861 (1979).

[47] A. Chutjian and S. K. Srivastava, J. Phys. B **8**, 2360 (1975).

[48] A. Chutjian, J. Phys. B **8**, 2360 (1975).

[49] C. B. Opal and E. C. Beaty, J. Phys. B **5**, 627 (1972).

[50] A. Yagishita, T. Takayanagi, and H. Suzuki, J. Phys. B **9**, L53 (1976).

[51] M. A. Dillon and E. N. Lassettre, J. Chem. Phys. **62**, 2373 (1975).

[52] M. A. Dillon, J. Chem. Phys. **63**, 2035 (1975).

[53] R. McAdams, M. T. Hollywood, A. Crowe, and J. F. Williams, J. Phys. B **13**, 3691 (1980).

[54] N. C. Steph and D. E. Golden, Phys. Rev. A **27**, 1678 (1983).

[55] H. B. van Linden van den Heuvell, J. van Eck, and H. G. M. Heideman, J. Phys. B **15**, 3517 (1982).

[56] P. A. Neill and A. Crowe, J. Phys. B **21**, 1879 (1988).

[57] P. A. Neill, B. P. Donnelly, and A. Crowe, J. Phys. B **22**, 1417 (1989).

[58] D. C. Cartwright and G. Csanak, J. Phys. B **19**, L485 (1986).

[59] B. P. Donnelly, P. A. Neill, and A. Crowe, J. Phys. B **21**, L321 (1988).

[60] B. P. Donnelly, D. T. McLaughlin, and A. Crowe, J. Phys. B **27**, 319 (1994).

[61] M. Eminyan, K. B. McAdam, J. Slevin, and H. Kleinpoppen, J. Phys. B **7**, 1519 (1974).

[62] D. T. McLaughlin, B. P. Donnelly, and A. Crowe, Z. Phys. D **29**, 259 (1994).

[63] A. G. Mikosza, R. Hippler, J. B. Wang, and J. F. Williams, Z. Phys. D **30**, 129 (1994).

[64] H. Batelaan, J. van Eck, and H. G. M. Heideman, J. Phys. B **24**, L397 (1991).

[65] H. J. Beyer, H. A. Silim, and H. Kleinpoppen, in *XVI International Conference on the Physics of Electronic and Atomic Collisions, Abstracts*, edited by A. Dalgarno, R. S. Freund, P. M. Koch, M. S. Lubell, and T. B. Lucatorto (Academic Press, New York, 1989), p. 165.

[66] J. P. Beijers, D. H. Madison, J. van Eck, and H. G. M. Heideman, J. Phys. B **20**, 167 (1987).

[67] M. Eminyan et al., J. Phys. B **8**, 2058 (1975).

[68] M. T. Hollywood, A. Crowe, and J. F. Williams, J. Phys. B **12**, 819 (1979).

[69] J. Slevin et al., J. Phys. B **13**, 3009 (1980).

[70] R. McAdams and J. F. Williams, J. Phys. B **15**, L247 (1982).

[71] D. H. Madison (private communication).